
A Cyberattack Detection-Isolation Scheme For CAV Under Changing Driving Environment

A PREPRINT

Sanchita Ghosh¹, Nutan Saha², and Tanushree Roy¹

¹Department of Mechanical Engineering, Texas Tech University, Lubbock, TX 79409, US.

Emails: sancghos@ttu.edu, tanushree.roy@ttu.edu.

²Department of Electrical Engineering, Veer Surenda Sai University of Technology, Odisha 768018, India.

Emails: nsaha_ee@vssut.ac.in.

September 23, 2024

ABSTRACT

Under a changing driving environment, a Connected Autonomous Vehicle (CAV) platoon relies strongly on the acquisition of accurate traffic information from neighboring vehicles as well as reliable commands from a centralized supervisory controller through the communication network. Even though such modalities are imperative to ensure the safe and efficient driving performance of CAVs, they led to multiple security challenges. Thus, a cyberattack on this network can corrupt vehicle-to-vehicle (V2V) and vehicle-to-infrastructure (V2I) communication, which can lead to unsafe or undesired driving scenarios. Hence, in this paper, we propose a cyberattack detection-isolation algorithm comprised of a unified V2V and V2I cyberattack detection scheme along with a V2I isolation scheme for CAVs under changing driving conditions. The proposed algorithm is constructed using a bank of residual generators with Lyapunov function-based performance guarantees, such as disturbance-to-state stability, robustness, and sensitivity. Finally, we showcase the efficacy of our proposed algorithm through extensive Monte-Carlo simulations using real-world highway and urban driving data. The results show that the proposed algorithm can enhance the cybersecurity of CAVs by detecting cyberattacks on CAV platoons and isolating infrastructure-level traffic manipulation.

1 Introduction

CAVs are gradually becoming an essential part of modern transportation by providing improved efficiency, safety, and energy sustainability [1, 2]. On the other hand, Vehicular Ad-hoc NETWORK (VANET) is one of the most explored technologies that can support these V2X communications (vehicle-to-everything i.e. both V2V and V2I) along with several facilities, and protocols to enable reliable operation of these Intelligent Transportation Systems (ITS) under changing traffic environments [3, 4] and can transmit local information including emergency warnings [5]. While the incorporation of this safety-critical information is crucial for effective platoon control, this also enhances the potential for cyberattacks on these networks [6, 7]. Thus, the task of detecting these cyberthreats in CAVs is crucial and such detection is especially challenging when the mode of operations is changing [8].

Most importantly, VANETS are utilized by vehicle platoons with cooperative adaptive cruise control (CACC) to ensure string stability. Here string stability refers to the reduction of traffic density disturbances during its upstream propagation [9]. To achieve this, each vehicle in the platoon relies on the V2X communication and on its onboard controller. The latter receives data from the preceding vehicle (V2V communication) and from the infrastructure (V2I communication) through a wireless communication network. Using this data along with the onboard sensor measurements (e.g. LiDAR, RADAR), it changes the vehicle's velocity to maintain a desired inter-vehicle distance, namely headway. The V2V communication in CACC enables the vehicle platoon to maintain a smaller headway among each other and thereby increasing the traffic flow [10]. Now, these optimum headways and vehicle velocities are not fixed for different driving or traffic environments. For example, generally on the interstates the platoon headway can be

kept smaller with higher velocities since traffic is mostly uninterrupted. Such strategies are used in truck platooning to increase fuel efficiency [11]. Conversely, for urban traffic, the headway is mostly larger with slower traffic speeds to avoid collisions during frequent stop-and-go conditions. Thus, such vehicle platoons must operate under different driving “modes” with changing driving environments [12].

Now, the goal for this paper is to ensure safety and string stability while accommodating these changes in the driving environment of the platoon. In particular, the V2I communication facilitates adapting to changing traffic conditions with updated information from global traffic data. Various methods such as machine learning-based classifiers, and dynamic programming are used to determine these driving modes via driving pattern recognition [12–14]. To ensure the string stability of the platoon and optimal energy consumption, different controller gains are designed for the vehicles under these different driving conditions [15]. The traffic infrastructure uses the V2I network to communicate with the onboard vehicular controllers to switch between these different gains or driving modes. In practice, the infrastructure uses Global Navigation Satellite System (GNSS) or Visual Positioning Systems (VPS) based data to obtain the trajectory of each vehicle and also to ascertain the changing driving conditions [12, 14]. We note here that various other modalities such as traffic reporting services, and social data [16, 17] can be also used to ascertain such changes in driving conditions. These redundancies are generally practiced to improve traffic safety [18].

Next, to understand the vulnerabilities of VANETS to cyberattacks, we note the structure of a typical VANET consists of a Road-Side Unit (RSU) and an On-Board Unit (OBU). These RSUs are installed on the roadside infrastructure and are responsible for providing local information and actuation signals to vehicles. These can be physically accessed by adversary employees during maintenance to get physical data and tamper the hardware [19]. Meanwhile, OBUs are installed on vehicles to receive the sensor data and the transmitted information from RSUs through wireless devices. Moreover, VANET can be configured to change communication topology between communicating vehicles as well as with the local RSUs [19, 20]. This further enhances the susceptibility of platoons to unsafe or undesirable operations. Occasionally, under VANET, a Dedicated Short Range Communication (DSRC) protocol is used and the U.S. Federal Communications Commission has allocated 75 MHz of licensed spectrum in the 5.9 GHz band for ITS [21]. Even though this short-range communication improves VANET security against long-range and stationary attackers, yet it fails to secure the vehicular network completely [22].

Hence, in this paper, we consider the possibility of cyberattacks through the compromised V2V and V2I wireless networks. While attacks on both of these networks can lead to unsafe or undesirable scenarios such as rear-end collisions [23], CACC disengagement [24], traffic congestion [25], etc., the V2I communication safety and privacy are remarkably more significant since every vehicle discloses its identity and tracking data [26]. Consequently, while an attack on the V2V channels explicitly impacts individual or adjacent vehicles in the platoon, an attack on the V2I network compromises the communications between all vehicles and critical infrastructure components (such as ramp metering, RSUs, etc.) and hence poses a potential threat for a wide-spread disruption in the whole traffic system [27]. For example, the adversary can use the V2I network to send tailor-made signals to multiple CAV platoons to create scenarios like bottleneck traffic cognition, stop-go traffic, and so on [28]. Moreover, (under a changing driving environment scenario) a cyberattack on the V2I channels mimics a compromised switching attack scenario and such an attack exhibits a high likelihood of leading the system to an unsafe operating region [29]. Thus, it is important to isolate the attacks on the V2I channel, if possible [30]. To address these threats, we categorize cyberattacks as V2V and V2I attacks [30–33]. Additionally, the V2X attack denotes either concurrent or asynchronous V2V-V2I attacks [34]. Thus we propose a unified diagnosis scheme to first detect the presence of V2V and/or V2I attacks and then, an isolation scheme to distinguish V2I attack scenarios.

2 Related Literature And Contribution

Existing CAV security and cyberattack detection can be broadly classified into (i) information-based, (ii) machine learning-based, and (iii) model-based approaches. In the information-based safety analysis, authors focused mainly on secured networks and data transmission [22, 35, 36] along with authentication and plausibility confirmation of data received through vehicular networks [37–39]. Similarly, in [36], authors proposed a data-encryption scheme to achieve reliable vehicle platoon operation. To enhance security while ensuring flexibility and programmability of the network, several works focused on software-defined network (SDN) [5, 20, 40]. Separating the centralized control panel from the data panel and the dynamic updating makes SDN more secure against cyberthreats [40]. However, when these informatics-based security measures are breached, the adversary poses severe risks to the vehicle platoon by gaining access to physical control [39].

Furthermore, several works focus on machine learning-based techniques to detect cyberattacks on CAVs. For example, a convoluted neural network (CNN) based detector is proposed in [41] to detect multi-source anomalies as well as single-source anomalies in sensor behavior. Thus the proposed solution is not restrictive to the detection in specific

scenarios only. Likewise, the authors proposed a reinforced learning-based data trust model to improve data authenticity in [42]. In [33], authors utilized expectation maximization (EM) and cumulative summation (CUSUM) algorithms to ensure real-time detection of V2I cyberattacks. Additionally, in [32], different driving environments are considered as a parameter during ML-based model training for the V2V attack detection strategy. However, these approaches rely heavily on the availability of data [4] and it is particularly difficult to train such classifier-based detectors when data generated by CAVs is limited and incomplete [43]. With increasing connectivity among smart infrastructures, the potential attack vectors increase proportionally, which in turn increases the occurrence of novel forms of attack on CAVs. Thus, limited data severely handicaps machine learning-based strategies [43], particularly in the context of new or unknown attacks [44].

In contrast, model-based approaches employ state estimation of the vehicle platoon using mathematical models of CAVs, to detect any deviation in the behavior of the CAVs from the nominal operation and consequently detect cyberattacks [45]. For instance, [46] proposed a Kalman filter-based (KF) detection scheme for an ego vehicle under a compromised controller by utilizing the measurements from neighboring vehicles. Likewise, an extended KF observer is used to detect cyberattacks under communication delay in [47]. Additionally, adaptive resilient observer-based distributed detectors are used to isolate between compromised and healthy vehicle sensors [48]. A per-vehicle detection scheme consisting of two ellipsoidal sets, namely a state prediction set and a state estimation set, is proposed in [49]. This method ensures the detection of both V2V and V2I attacks. Moreover, along with the system model and control-based tools, authors utilized the redundancies among the physical signals and the social signals received from users' mobile and social media to detect cyberattacks on connected transportation systems in [50]. Similarly, sensor information redundancies were exploited to isolate the compromised vehicles under Syb attacks in [51]. [52] proposed a detection algorithm scheme for Denial-of-Service (DoS) attacks on the communication network by means of sliding mode and adaptive observers for individual vehicles and estimated the impact of the attack on CAV. Finally, an integrated framework combining CNN and KF was proposed in [4] to detect anomalous sensors for CAV platoons.

Nevertheless, these works considered a single control law for all driving conditions, although multi-mode control strategy in CAVs is essential to ensure optimal operation such as energy efficiency, vehicle safety, etc. under changing driving environments [12, 53]. Moreover, these works did not consider isolating V2I attack scenarios, where the latter introduces a variety of vulnerabilities, including exposed infrastructure data access and large-scale resource disruption [27]. Furthermore, identification of single or multiple compromised vehicles is often unaddressed in many of these works, which can enable the authorities to respond with proper countermeasures knowing the source and nature of the attacks. Therefore, to address these research gaps, in this paper our contributions are as follows:

- We propose a detection-isolation algorithm based on residual generation to detect both V2V and V2I (i. e. V2X) attacks in a CAV platoon traveling under different modes depending on the changing driving environment.
- The proposed algorithm can also isolate the attacks on the V2I channel without restrictions on the attack policies.
- The proposed algorithm can identify the compromised vehicles and thus track down the source of the attack.
- The efficacy of the algorithm is tested using realistic driving patterns from NGSIM (Next-Generation Simulation) and UDDS (Urban Dynamometer Drive Schedules) data.

The rest of the paper is organized as follows. In Section 3, we present the problem formulation including the closed-loop system model of the CAV under consideration. Section 4 presents the proposed V2X detection scheme and mathematical analysis to obtain necessary and sufficient conditions for performance guarantees. Next, a V2I isolation scheme is presented in Section 5. The simulation results showing the effectiveness of our proposed algorithm to detect V2X attacks as well as to isolate V2I attacks are presented in Section 6. Finally, we present the concluding remarks in Section 7.

Notation: In this paper, we used \mathbb{R} to denote the set of natural numbers. The Euclidean norm of a vector $\|x\|_2 = \sqrt{x^T x}$, and the \mathcal{L}_2 norm of a vector-valued function $\|x\|_{\mathcal{L}_2} := \sqrt{\left(\int_0^\infty \|x\|_2^2 dt\right)}$. The absolute value of the variable a is denoted as $|a|$. We used I_a to denote an identity matrix. To denote the minimum and maximum eigenvalue of a matrix A , we used $\lambda_{\min[A]}$ and $\lambda_{\max[A]}$ respectively. \dot{f} denotes derivative with respect to t i.e. $\dot{f} = \frac{df}{dt}$. For two vectors x, y , and a matrix A , we define a binary quadratic function $q(x, A, y) = x^T A y + y^T A^T x$.

3 Problem Formulation

Let us consider a vehicle platoon under CACC with V2V and V2I communication. The vehicle platoon runs with different operating modes to cope with changing driving environments. The leader vehicle drives in response to the surrounding driving environment. We note here that the leader vehicle is either human-driven or semi-autonomous which is auspicious in practical implementation [54]. A supervisory controller monitors the trajectory, position, and acceleration of the leader vehicle to decide upon the appropriate operational mode for the rest of the vehicle platoon [55]. It communicates this information to the onboard vehicular controllers of the follower vehicles to switch among different “modes”. We note here that each mode corresponds to specific controller gains. These different gains along with the V2V and V2I data ensure the string stability of the platoon. In this paper, we assume that the infrastructure uses GNSS-based data to obtain the trajectory and position data of each vehicle. Fig. 1 shows the block diagram of our problem framework.

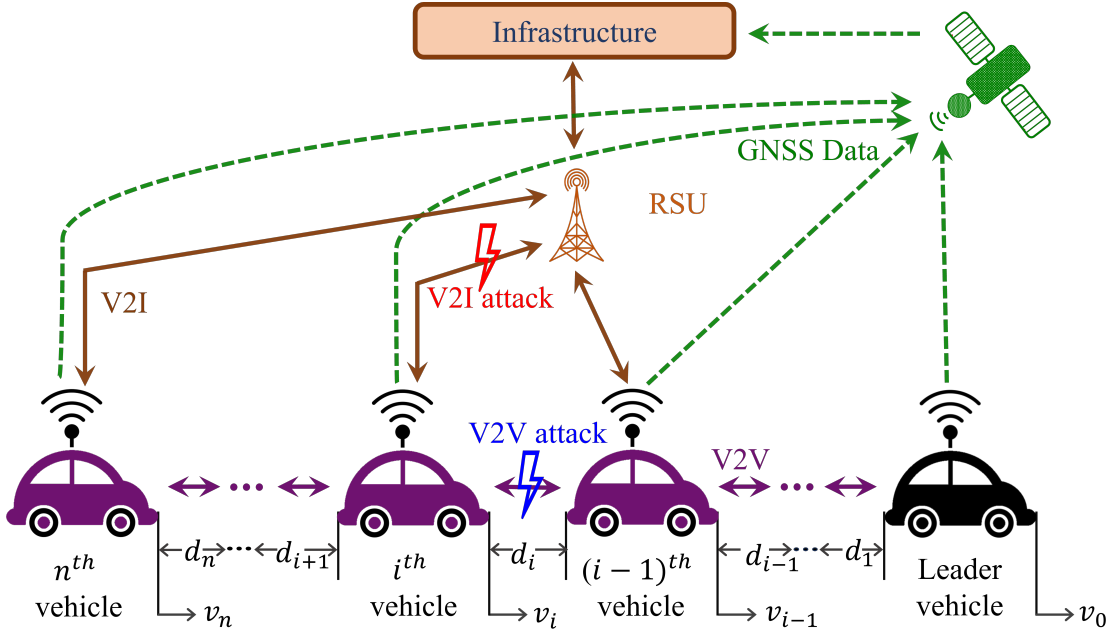


Figure 1: Block diagram of the vehicle platoon.

Assumption 1. In this problem setting, we assume that the traffic measurements from the GNSS or VPS are not simultaneously compromised along with the communication network. Additionally, under nominal conditions, we are assuming a delay-free communication network. Generally, consideration of delays in traffic measurements results in a relatively slower detection time [56] and will be considered in our future work.

Remark 1. The human-driven or semi-autonomous leader vehicle of the CAV platoon is not susceptible to cyberattacks. Yet, if the leader vehicle is a CAV, we will still be able to extend our framework and detect-isolate cyberattacks on the leader vehicle (in the near future), as long as we can collect the positional data of the vehicle preceding the leader. In the unlikely event that such information is unavailable, our algorithm in its present form will be unable to detect the cyberattack on the leader and such scenarios remain beyond the scope of our current work.

3.1 Closed-loop vehicle dynamics

We consider a car following (CF) vehicle platoon with a string of $n + 1$ vehicles. First, let us define the state vector for the leader vehicle as $\bar{z}_0 = [x_0 \ v_0]^T$ where x_0, v_0 are respectively the position and velocity of the leader vehicle. The vehicle dynamics of the leader vehicle can be written as $\dot{\bar{z}}_0 = A_0 \bar{z}_0 + B_0 u_0, t \geq 0$, Here the state matrix $A_0 \in \mathbb{R}^{2 \times 2}$ is defined as $A_0 = \begin{bmatrix} 0 & 1 \\ 0 & 0 \end{bmatrix}$. The input matrix $B_0 \in \mathbb{R}^{2 \times 1}$ is defined as $B_0 = \begin{bmatrix} 0 \\ 1 \end{bmatrix}^T$. The input $u_0 \in \mathbb{R}^1$ is defined as $u_0 = a_0$. a_0 is the acceleration for the leader vehicle. Let $i \in \{0, 1, \dots, n\}$ represent the vehicle number in the platoon where $i = 0$ represents the leader vehicle. The rest n numbers of follower vehicles are expected to follow their preceding vehicle at a desired headway h_{d_i} , which is defined as $h_{d_i} = s_i + \mathcal{T}_\alpha v_i, 1 \leq i \leq n$, where s_i is the standstill distance for i^{th} vehicle and \mathcal{T}_α is the time headway during α^{th} operating mode. v_i is the velocity of the i^{th}

vehicle. Here the piece-wise constant switching signal $\alpha : [0, \infty) \rightarrow \mathcal{M} = [1, 2, \dots, m]$ from infrastructure indicates the operational mode of the system. The platoon is assumed to be homogeneous and therefore the time headway \mathcal{T}_α is not dependent on the vehicle i . The actual headway between vehicle i and the preceding vehicle $i-1$ is denoted as h_i . Now, let us define state vector $z_i = [h_i \quad v_i \quad a_i]^T$, where a_i is the acceleration of the i^{th} vehicle. We then re-write the state vector of the leader vehicle as $z_0 = [0 \quad v_0 \quad a_0]^T$. Then the closed-loop vehicle dynamics of the i^{th} vehicle becomes

$$\dot{z}_i = Az_i + Dz_{i-1} + Bu_i + \bar{w}_i, \quad y_i = Cz_i, \quad 1 \leq i \leq n \quad (1)$$

$$\dot{u}_i = -k_{u_\alpha} u_i + A_{c_\alpha} z_i + D_{c_\alpha} z_{i-1} - H_\alpha s_i + \frac{\theta_i}{\mathcal{T}_\alpha} u_{i-1}. \quad (2)$$

Here $A, D \in \mathbb{R}^{3 \times 3}$, $B \in \mathbb{R}^{3 \times 1}$, $A_{c_\alpha}, D_{c_\alpha} \in \mathbb{R}^{1 \times 3}$, and $H_\alpha \in \mathbb{R}^1$ are considered identical for all vehicles following the homogeneous platoon assumption and are defined as

$$\begin{aligned} A &= \begin{bmatrix} 0 & -1 & 0 \\ 0 & 0 & 1 \\ 0 & 0 & -\frac{1}{\Sigma} \end{bmatrix}, \quad A_{c_\alpha} = \frac{k_\alpha}{\mathcal{T}_\alpha} \begin{bmatrix} 1 & -\mathcal{T}_\alpha & 0 \\ 0 & -1 & -\mathcal{T}_\alpha \\ 0 & 0 & \frac{\mathcal{T}_\alpha}{\Sigma} - 1 \end{bmatrix}, \\ D &= \begin{bmatrix} 0 & 1 & 0 \\ \mathbf{0} & \mathbf{0} & \mathbf{0} \end{bmatrix}, \quad D_{c_\alpha} = \frac{k_\alpha}{\mathcal{T}_\alpha} \begin{bmatrix} 0 & \mathbf{0} \\ \mathbf{0} & I \end{bmatrix}, \\ B &= [0 \quad 0 \quad \frac{1}{\Sigma}]^T, \quad H_\alpha = \frac{k_\alpha}{\mathcal{T}_\alpha} [1 \quad 0 \quad 0]^T. \end{aligned} \quad (3)$$

The parameter Σ is the time constant to represent the engine dynamics of the vehicle, $y_i \in \mathbb{R}^q$ ($q \leq 3$) is the output and $u_i \in \mathbb{R}^1$ is the controlled input. $C \in \mathbb{R}^{q \times 3}$ is the output matrix. $\bar{w}_i \in \mathbb{R}^3$ is the uncertainty. $k_\alpha \in \mathbb{R}^{1 \times 3}$ is the controller gain vector defined as $k_\alpha = [k_{p_\alpha} \quad k_{d_\alpha} \quad k_{dd_\alpha}]$ and $k_{u_\alpha} = \frac{1}{\mathcal{T}_\alpha} + \frac{k_{dd_\alpha}}{\Sigma}$. The function $\theta_i : [0, \infty) \rightarrow \{0, 1\}$ represents the V2V communication where the values 0 and 1 indicate ceased or intact communication respectively.

To analyze the closed-loop vehicle dynamics, let us define an augmented state vector $\zeta_i = [z_i^T \quad u_i]^T$ which yields

$$\dot{\zeta}_i = \mathcal{A}_\alpha \zeta_i + \mathcal{D}_{\theta_\alpha} \zeta_{i-1} - \mathcal{H}_\alpha s_i + w_i, \quad y_i = \mathcal{C} \zeta_i, \quad (4)$$

where $\mathcal{A}_\alpha, \mathcal{D}_{\theta_\alpha} \in \mathbb{R}^{4 \times 4}$, $\mathcal{C} \in \mathbb{R}^{q \times 4}$, and $\mathcal{H}_\alpha, w_i \in \mathbb{R}^{4 \times 1}$ are defined as

$$\begin{aligned} \mathcal{A}_\alpha &= \begin{bmatrix} A & B \\ A_{c_\alpha} & -k_{u_\alpha} \end{bmatrix}, \quad \mathcal{D}_{\theta_\alpha} = \begin{bmatrix} D & \mathbf{0} \\ D_{c_\alpha} & \frac{\theta_i}{\mathcal{T}_\alpha} \end{bmatrix}, \quad \mathcal{C} = \begin{bmatrix} C^T \\ \mathbf{0} \end{bmatrix}^T, \\ \mathcal{H}_\alpha &= [\mathbf{0} \quad H_\alpha]^T, \quad w_i = [I \quad \mathbf{0}]^T \bar{w}_i. \end{aligned} \quad (5)$$

Assumption 2. *The switching between the operational modes of the CAV platoon is assumed to be significantly slow since the driving environment changes infrequently. In particular, we assume that such switching time is more than the average dwell time (ADT) [57] and the platoon/vehicles remain stable under the designed controller gains for each mode.*

3.2 Cyberattack policy and compromised platoon dynamics

In this framework, we consider that the adversary can simultaneously attack single or multiple follower vehicles of the platoon either through the V2V or through the V2I communication channel. An attack on both the V2V and the V2I communication (i.e. V2X) is possible as well. Here the primary objective of the adversary is to drive the platoon to unsafe or undesired conditions. In unsafe conditions, vehicles may run too close to each other (too small a headway distance) during the stop-go traffic condition. This can lead to a high probability of collisions as shown in the left plot of Fig. 2. On the other hand, a compromised vehicle may trail off if the headway distance is too large and the velocity is too small compared to the preceding vehicle, leading to disengaged CACC [24]. The right plot of Fig. 2 exhibits this scenario.

The adversary can opt for several active network attack policies such as DoS, distributed DoS (DDoS), blackhole, false-data-injection (FDI), and replay attacks to manipulate the platoon control policy and/or measurement (4). They particularly affect the control input dynamics in (2) [58]. Such attacks can be formulated with the switching command signal α_i and the V2V communication function θ_i along with the preceding vehicle's control input u_{i-1} to mathematically represent these different attack policies to better understand their impacts in the context of our framework. Furthermore, the compromised scenarios are denoted by $\tilde{\alpha}_i$ and $\tilde{\theta}_i \tilde{u}_{i-1}$. We define two Boolean scalars δ_α and δ_θ such that $\delta_\alpha, \delta_\theta = 1$ indicate the activation of V2V and V2I attacks, respectively.

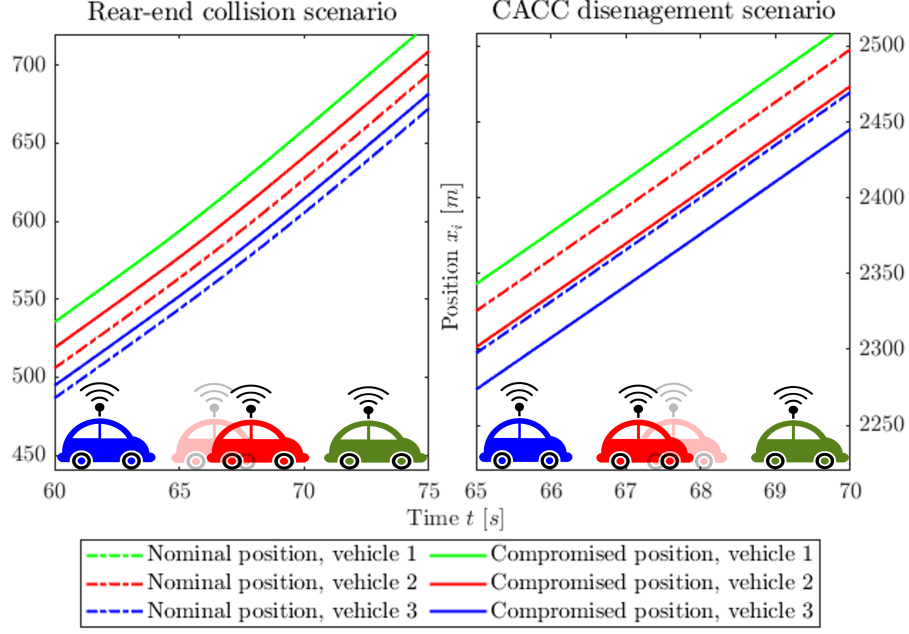


Figure 2: Objectives of the adversary.

DoS/DDoS Attack: During DoS attacks, the compromised vehicle stops receiving any updates from the infrastructure or/ and the preceding vehicle and hence, continues to run with the previous information [19]. Mathematically we define this scenario for the i^{th} vehicle as

$$\text{V2V attack: } \tilde{\theta}_i \tilde{u}_{i-1} = \theta_i (u_{i-1} - \delta_\theta [u_{i-1} - u_{i-1}(t_0)]), \quad (6)$$

$$\text{V2I attack: } \tilde{\alpha}_i = \alpha_i - \delta_\alpha [\alpha_i - \alpha_i(t_0)], \quad (7)$$

where the attacks begin at time t_0 . Multiple vehicles are corrupted during the DDoS attack, i. e. these V2X communications can be halted for more than one vehicle.

False Data Injection (FDI): In this scenario, the adversary provides the compromised vehicle/s with the information to switch to a wrong controller mode during a V2I attack. Conversely, during a V2V attack the adversary provides wrong u_{i-1} information. Hence, we define this scenario as follows.

$$\text{V2V attack: } \tilde{\theta}_i \tilde{u}_{i-1} = \theta_i (u_{i-1} - \delta_\theta [u_{i-1} - \bar{u}_{i-1}]), \quad (8)$$

$$\text{V2I attack: } \tilde{\alpha}_i = \alpha_i - \delta_\alpha [\alpha_i - \bar{\alpha}_i]; \bar{\alpha}_i \in \mathcal{M} \setminus \{\alpha_i\}. \quad (9)$$

An example of FDI is the Blackhole attack where the compromised vehicle ceases any upstream information flow [59].

Replay Attack: This is a two-phase attack. First, the adversary stores the switching command signals α or/ and the preceding vehicle's control input u_{i-1} for a time interval $[t_0 - \Delta\tau, t_0]$. Then in the next phase, the adversary starts to replay the stored commands in a loop. Thus, for $t_a = t - \Delta\tau$, the final attack can be represented as

$$\text{V2V attack: } \tilde{\theta}_i \tilde{u}_{i-1} = \theta_i (u_{i-1} - \delta_\theta [u_{i-1} - u_{i-1}(t_a)]), \quad (10)$$

$$\text{V2I attack: } \tilde{\alpha}_i = \alpha_i - \delta_\alpha [\alpha_i - \alpha_i(t_a)]. \quad (11)$$

Hence, we define the V2V and V2I attacks concisely as

$$\tilde{\theta}_i \tilde{u}_{i-1} = \theta_i u_{i-1} - \Delta_\theta; \quad \tilde{\theta}_i : [0, \infty) \rightarrow \{0, 1\}, \quad (12)$$

$$\tilde{\alpha}_i = \alpha_i - \Delta_\alpha; \quad \tilde{\alpha}_i : [0, \infty) \rightarrow \mathcal{M} = \{1, 2, \dots, m\}. \quad (13)$$

Here, $\Delta_\alpha, \Delta_\theta$ are defined such that they indicate the presence of any cyberattacks when $\delta_\alpha, \delta_\theta \neq 0$. Now, comparing (13) with standard compromised switching attack definition [29], we can deduce that the V2I cyberattacks are in fact compromised switching attacks for the platoon, and thus, the compromised vehicles run with mismatched controllers. On the other hand, during a V2V attack the compromised vehicles run with the correct controller, however track

a wrong desired acceleration. Accordingly, the V2I attacks appear as multiplicative anomalies in the closed-loop vehicle dynamics in terms of $\mathcal{A}_{\tilde{\alpha}}, \mathcal{D}_{\theta\tilde{\alpha}}, \mathcal{H}_{\tilde{\alpha}}$ and the V2V attacks appear as additive anomalies as $\mathcal{D}_{\tilde{\theta}\tilde{\alpha}}\tilde{u}_{i-1}$.

Thus, we utilize the standard methods [60] to convert the multiplicative anomalies to additive anomalies. However, the three possible cases namely only V2V, only V2I, and simultaneous V2V-V2I attacks affect the platoon dynamics differently. Therefore, the compromised platoon dynamics is re-written as

$$\begin{aligned} \dot{\zeta}_i &= \mathcal{A}_{\alpha}\zeta_i + \mathcal{D}_{\theta\alpha}\zeta_{i-1} - \mathcal{H}_{\alpha}s_i + E_{\theta i}f_{\theta i} + E_{\alpha i}f_{\alpha i} \\ &+ E_{\theta\alpha i}f_{\theta\alpha i} + w_i, \quad \zeta_i(0) = \zeta_{i0}, \quad t \geq 0. \end{aligned} \quad (14)$$

$E_{\theta i}, E_{\alpha i}, E_{\theta\alpha i}$ are the known matrices and $f_{\theta i}, f_{\alpha i}, f_{\theta\alpha i}$ are the unknown time functions representing respectively only V2V, only V2I, simultaneous V2V-V2I attacks such that $\mathcal{A}_{\tilde{\alpha}}\zeta_i + \mathcal{D}_{\tilde{\theta}\tilde{\alpha}}\tilde{\zeta}_{i-1} - \mathcal{H}_{\tilde{\alpha}}s_i = \mathcal{A}_{\alpha}\zeta_i + \mathcal{D}_{\theta\alpha}\zeta_{i-1} - \mathcal{H}_{\alpha}s_i + E_{\theta i}f_{\theta i} + E_{\alpha i}f_{\alpha i} + E_{\theta\alpha i}f_{\theta\alpha i}$. In other words $\Delta_{\theta} \neq 0$ implies $f_{\theta i} \neq 0$, $\Delta_{\alpha} \neq 0$ implies $f_{\alpha i} \neq 0$, and $\Delta_{\theta}, \Delta_{\alpha} \neq 0$ implies $f_{\theta i}, f_{\alpha i}, f_{\theta\alpha i} \neq 0$. Considering the closed-loop vehicle platoon dynamics (14), we now introduce our proposed algorithm.

3.3 Cyberattack detection-isolation algorithm

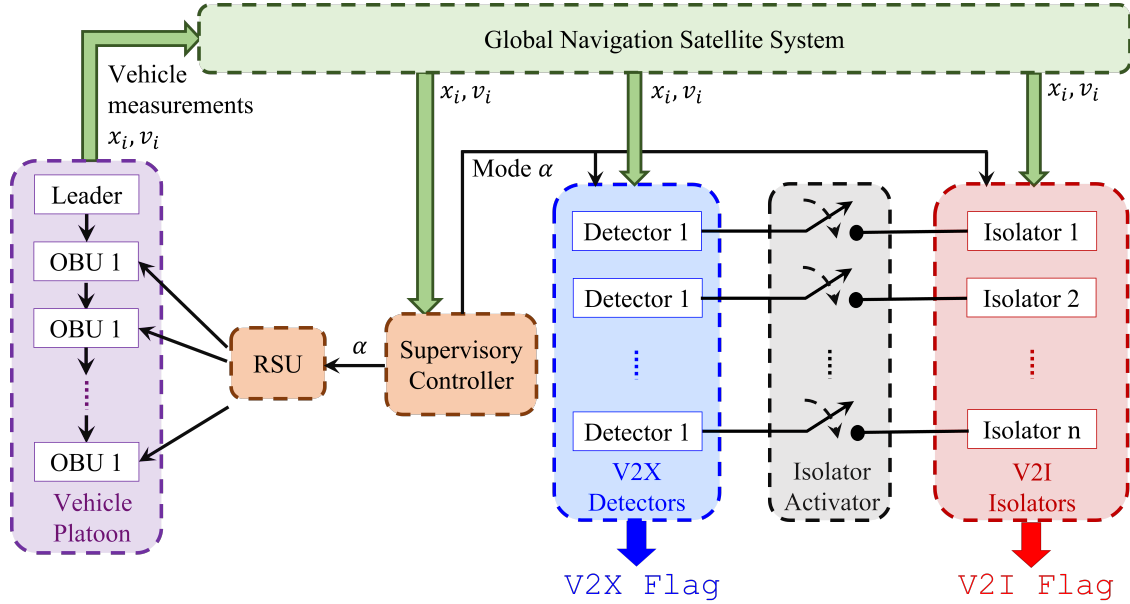


Figure 3: Schematic block diagram of the detection-isolation algorithm.

The objective of our proposed two-phase algorithm is to detect the presence of any V2X cyberattacks and thereafter isolate the presence of V2I attacks. The first phase is the V2X detection scheme (DS) which monitors individual vehicle performance for any deviation from the desired behaviors. Such deviations are captured by the V2X DS residual and a V2X attack is detected when the V2X DS residual crosses a threshold. Upon detection of a V2X cyberattack in a vehicle, a V2X flag is generated and the corresponding second phase of the algorithm is activated for that vehicle. This is the V2I isolation scheme (IS). Similar to the first phase, the V2I IS investigates individual vehicle performance to generate a V2I flag if the performance deterioration is due to a V2I attack and hence the V2I IS residual crosses a threshold. To achieve this goal, we consider a bank of n number of switched-mode detectors corresponding to the n follower vehicles of the platoon. All of these $2n$ detectors and isolators have m operational modes corresponding to the m operational modes of the vehicle platoon. Similarly, all the n detectors and isolators run with the same mode α at a time and receive the mode information from the supervisory controller. The proposed detection-isolation algorithm is shown as a schematic diagram in Fig. 3.

Furthermore, the V2X DS and the V2I IS should be robust to uncertainties that may arise from the unmodeled system dynamics or measurement noises. Contrarily, they must remain sensitive to cyberattacks that are specifically crafted by an adversary to drive the system towards unsafe or undesired states. Therefore, we designed all the detector and isolator gains to ensure the following performance guarantees [29]:

Disturbance-to-state stable (DSS): DSS refers to the condition, where for any driving mode α for a vehicle, the residual for the detector/isolator must remain bounded under bounded V2V and/or V2I attack and under bounded uncertainties.

Robustness: To ensure robustness, the gains must be chosen such that the effect of the uncertainties on the residual is suppressed by a robustness factor (RF), which must be minimized.

Sensitivity: Conversely, we want to choose the gains such that it amplifies the effect of every attack by a sensitivity factor (SF), which must be maximized.

Remark 2. *RF and SF cannot be arbitrarily minimized or maximized simultaneously since their impact on the gain is opposite. For a given gain, if SF is maximized, the algorithm will be highly sensitive to both attacks and uncertainties. This increases the probability of attack detection as well as the probability of invalid flag generation due to uncertainties leading to false alarms. Conversely, if the RF is kept small, then the algorithm will be less sensitive and more robust to uncertainties while suffering from a high chance of missed detection in presence of cyberattacks. Consequently, we use an optimization scheme to address this robustness-sensitivity trade-off. Specifically, we utilize the optimization weighting constant to prioritize between these two factors and thus, to obtain an appropriate balance between the robustness and the sensitivity of the algorithm. Lastly, we note that the robustness-sensitivity balance varies with the design criteria of preferred uncertainty tolerance and detectable attack magnitude. It remains unaffected by the complexity and patterns of cyberattacks and thus, will be effective for new and emerging attacks of appropriate magnitude.*

4 V2X Detection Scheme

In this section, we first present the V2X detector dynamics and then obtain the design conditions in the form of linear matrix inequalities (LMIs) to ensure the desired performance.

4.1 V2X detector dynamics

Let us first define the augmented detector dynamics (15), $\forall i \in \{1, 2, \dots, n\}$ considering the system model (14) such that the detector i corresponds to the i^{th} vehicle of the platoon.

$$\dot{\hat{\zeta}}_i = \mathcal{A}_\alpha \hat{\zeta}_i + \mathcal{D}_{\theta\alpha} \hat{\zeta}_{i-1} - \mathcal{H}_\alpha s_i + \mathcal{L}_\alpha (y_i - \hat{y}_i), \quad \hat{y}_i = \mathcal{C} \hat{\zeta}_i. \quad (15)$$

Here $\hat{\zeta}_i \in \mathbb{R}^4$ and $\hat{y}_i \in \mathbb{R}^q$ are detector state and output respectively. $\mathcal{L}_\alpha \in \mathbb{R}^{4 \times q}$ is the detector gain matrix to be designed. We note here that \mathcal{L}_α is the same for each detector due to the homogeneity assumption on the platoon.

4.2 Error dynamics and V2X DS residual generation

The error between the platoon dynamics and the detector dynamics is defined as $e_i = \zeta_i - \hat{\zeta}_i$. Thus, from (14) and (15) the error dynamics can be written as

$$\begin{aligned} \dot{e}_i = & [\mathcal{A}_\alpha - \mathcal{L}_\alpha \mathcal{C}] e_i + \mathcal{D}_{\theta\alpha} e_{i-1} + E_{\theta i} f_{\theta i} \\ & + E_{\alpha i} f_{\alpha i} + E_{\theta\alpha i} f_{\theta\alpha i} + w_i. \end{aligned} \quad (16)$$

Since the deviation in headway indicates the possibility of extreme scenarios such as rear-end collisions or CACC disengagement, the detector output r_i is defined as

$$r_i = h_i - \hat{h}_i = N e_i, \quad (17)$$

where \hat{h}_i is the estimated headway and $N = [1 \ 0 \ 0 \ 0] \in \mathbb{R}^{1 \times 4}$. We note here that (16) indicates that the proposed DS (15) is impacted by the preceding vehicle's error e_{i-1} . Therefore, we define the generated V2X DS residual, $r_{c,i}$ as

$$r_{c,i} = \max \left(0, \left[\|r_i\|_2^2 - \|e_{i-1}\|_2^2 \right] \right). \quad (18)$$

4.3 Detector gain design

Table 1 enlists the definitions of necessary constants and matrices to state the LMI criteria for the detector gain matrix \mathcal{L}_α to ensure the desired performance in Theorem 1.

Constants and matrices utilized in Theorem 1	
$\gamma_{1i} = -\min_{\alpha} \frac{\lambda_{\min}[\Lambda_{1\alpha i}]}{\lambda_{\min}[N^T N]}$	$\rho_{2i} = \frac{\rho_{4i}}{\rho_{3i}}$
$\mathfrak{N} = N^T P_{\alpha} N$	$\mathcal{W}_{\alpha i} = \begin{bmatrix} P_{\alpha} N \mathcal{D}_{\theta \alpha} & P_{\alpha} N \end{bmatrix}$
$F_{\alpha i} = \begin{bmatrix} P_{\alpha} N \mathcal{D}_{\theta \alpha} & P_{\alpha} N E_{\alpha i} & P_{\alpha} N E_{\theta i} & P_{\alpha} N E_{\theta \alpha i} \end{bmatrix}$	
$\Lambda_{1\alpha i} = (\mathcal{A}_{\alpha} - \mathcal{L}_{\alpha} \mathcal{C})^T \mathfrak{N} + \mathfrak{N} (\mathcal{A}_{\alpha} - \mathcal{L}_{\alpha} \mathcal{C})$	
$\Lambda_{2\alpha i} = \Lambda_{1\alpha i} + \frac{1}{\beta_{1i}} \mathfrak{N} \mathcal{D}_{\theta \alpha} \mathcal{D}_{\theta \alpha}^T \mathfrak{N} + \frac{1}{\beta_{2i}} \mathfrak{N} E_{\alpha i} E_{\alpha i}^T \mathfrak{N}$ $+ \frac{1}{\beta_{3i}} \mathfrak{N} E_{\theta i} E_{\theta i}^T \mathfrak{N} + \frac{1}{\beta_{4i}} \mathfrak{N} E_{\theta \alpha i} E_{\theta \alpha i}^T \mathfrak{N} + \frac{1}{\beta_{5i}} \mathfrak{N} \mathfrak{N}$	
$\mathcal{G}_1 = \text{diag}[I, -I - \rho_{1i} I_4]$	
$\mathcal{G}_2 = \text{diag}[\rho_{3i} I, -\rho_{3i} I, -\rho_{4i} I_4, -\rho_{4i} I_4, -\rho_{4i} I_4]$	
$\mathcal{B}_{1\alpha i} = \begin{bmatrix} -\gamma_{1i} I & \mathcal{W}_{\alpha i} \\ \mathcal{W}_{\alpha i}^T & \mathbf{0} \end{bmatrix}$	$\mathcal{B}_{2\alpha i} = \begin{bmatrix} \gamma_{1i} I & F_{\alpha i} \\ F_{\alpha i}^T & \mathbf{0} \end{bmatrix}$

Table 1: List of required constants and matrices

Theorem 1. *Let us consider the vehicle platoon dynamics (14) and the V2X detector dynamics (15). The i^{th} detector is considered DSS, robust to uncertainty, and sensitive to cyberattacks for every mode α , if there exists a set of positive symmetric matrices $\mathcal{P} := \{P_{\alpha} : \alpha \in \mathcal{M}\}$ and constants $\rho_{j_i}, \beta_{j_i}, \gamma_{1i} > 0, \forall j \in \{1, 2, 3, 4\}$ and $0 \leq \mu_i \leq 1$, such that the constrained multi-objective optimization problem posed below has a feasible solution.*

$$\max_{\mathcal{L}_{\alpha}} [\mu_i(-\rho_{1i}) + (1 - \mu_i)\rho_{2i}], \quad \forall i \in \{1, 2, \dots, n\}; \quad (19)$$

$$\text{Subjected to } \Lambda_{2\alpha i} < 0, \quad (\text{DSS criteria}) \quad (20)$$

$$\mathcal{G}_1 + \mathcal{B}_{1\alpha i} \leq 0, \quad (\text{Robustness criteria}) \quad (21)$$

$$\mathcal{G}_2 - \mathcal{B}_{2\alpha i} \geq 0, \quad (\text{Sensitivity criteria}) \quad (22)$$

where $\Lambda_{2\alpha i}, \mathcal{G}_1, \mathcal{B}_{1\alpha i}, \mathcal{G}_2, \mathcal{B}_{2\alpha i}$ are defined in Table 1.

Proof. The proof is shown in the appendix. ■

Remark 3. *The DSS criteria ensure that the V2X DS residual $r_{c,i}(t)$ exponentially converges to zero under no cyberattacks and no uncertainties, i. e., $f_{\theta i}, f_{\alpha i}, f_{\theta \alpha i}, w_i = 0$. This proves the nominal exponential stability criteria for the V2X DS.*

Hence, from Theorem 1 we have obtained the LMI conditions for detector gains to ensure the performance benchmarks for the V2X DS. Next, we will define the V2X detector threshold to make an attack decision.

4.4 V2X attack decision and V2I IS activator

Each V2X DS residual generated from the n number of detectors is compared with a pre-defined threshold J_{DS} to make an attack detection. If the generated V2X DS residual $r_{c,i}$ (18) crosses the threshold J_{DS} , then a V2X attack decision is made and the second phase which is the V2I IS is activated. The threshold J_{DS} can be defined by observing the probability of the false alarm P_D corresponding to that specific threshold value, i. e., the probability of the residual $r_{c,i}$ crossing the threshold J_{DS} under nominal operation. First, we generate the V2X DS residual data r_w under no-attack and in presence of uncertainties scenarios ($\Delta_{\alpha}, \Delta_{\theta} = 0, w_i \neq 0$) from Monte-Carlo simulations. In practical application, we can test-run the vehicle platoon under different driving conditions such as urban, suburban, and highway routes at diverse time intervals within a day to collect the necessary V2X DS residual data r_w . Then, we can obtain the false alarm probability P_D as:

$$P_D = P(r_{c,i} > J_{DS} | \Delta_{\alpha} = 0 \& \Delta_{\theta} = 0) = \int_{J_{DS}}^{\infty} P(r_w) dr_w,$$

$r_{c,i} \geq J_{DS}$ implies V2X attack flag is generated for the i^{th} vehicle and simultaneous activation of V2I IS, otherwise there is no attack.

5 V2I Isolation Scheme

Upon V2X attack flag generation and V2I IS activation, it is confirmed that single or multiple vehicles are under cyberattacks that can show up in vehicle dynamics as 3 cases:

Case 1. *only V2V attack:* presence of $\tilde{\theta}_i \tilde{u}_{i-1}$ ($E_{\theta_i} f_{\theta_i}$) term,

Case 2. *only V2I attack:* presence of $\tilde{\alpha}_i$ ($E_{\alpha_i} f_{\alpha_i}$) term, and

Case 3. *simultaneous V2V-V2I attacks:* presence of both $\tilde{\theta}_i \tilde{u}_{i-1}$ and $\tilde{\alpha}_i$ ($E_{\theta_{\alpha_i}} f_{\theta_{\alpha_i}}$) terms.

Now our objective is to isolate the V2I attacks, i.e., presence of $\tilde{\alpha}_i$ in the event of Cases 2 and 3 with residual-based observers. To achieve this objective, the V2I IS acquires and utilizes the data transmitted through the V2V network channel. Thus, if the compromised i^{th} vehicle receives $\tilde{\theta}_i \tilde{u}_{i-1}$, the corresponding V2I IS model contains the same term. Hence, the incorporation of this V2V data essentially equips the V2I IS scheme with the ability to match both the nominal and corrupt V2V communication scenarios. Therefore, in the event of Case 1, the V2I IS residual never crosses the threshold.

Contrarily, in Cases 2 and 3, the V2I IS dynamics still run with expected mode α , while the compromised vehicle dynamics run with the compromised mode $\tilde{\alpha}_i$. This mismatch eventually drives the V2I IS residual to cross the threshold and an isolation flag is generated indicating the presence of V2I attack. Mathematically, the V2V information is given through f_{θ_i} , which is available to i -th V2I IS observer, while $f_{\alpha_i}, f_{\theta_{\alpha_i}}$ are still unknown to the observer. Thus, the V2I isolator dynamics is modeled following the system model (14) with the admitted V2V communication as

$$\begin{aligned} \dot{\hat{\xi}}_i &= \mathcal{A}_\alpha \hat{\xi}_i + \mathcal{D}_{\theta_\alpha} \hat{\xi}_{i-1} - \mathcal{H}_\alpha s_i + E_{\theta_i} f_{\theta_i} + \mathfrak{M}_\alpha (y_i - \hat{Y}_i), \\ \hat{Y}_i &= \mathcal{C} \hat{\xi}_i, \quad t \geq t_0; \quad \hat{\xi}_i(t_0) = \hat{\zeta}_i(t_0). \end{aligned} \quad (23)$$

Here $\hat{\xi}_i$, \hat{Y}_i , and \mathfrak{M}_α are respectively the isolator state, output, and gain matrix and t_0 is the time of V2X attack detection. We note here, $\hat{\xi}_{i-1}(t) = \hat{\zeta}_{i-1}(t)$ if the $(i-1)^{th}$ isolator is not activated. Now, the error between the system and the isolator dynamics is defined as $d_i := \zeta_i - \hat{\xi}_i$. From (14) and (23) and with $\mathcal{A}_{\mathfrak{M}_\alpha} = \mathcal{A}_\alpha - \mathfrak{M}_\alpha \mathcal{C}$, the error dynamics for the IS:

$$\dot{d}_i = \mathcal{A}_{\mathfrak{M}_\alpha} d_i + \mathcal{D}_{\theta_\alpha} d_{i-1} + E_{\alpha_i} f_{\alpha_i} + E_{\theta_{\alpha_i}} f_{\theta_{\alpha_i}} + w_i. \quad (24)$$

Now, we denote the generated residual from these V2I IS observers as *V2I IS residual* $\psi_i = h_i - \hat{H}_i = N d_i$. Here, \hat{H}_i is estimated headway under V2V attack. From (24), we can conclude that the generated V2I IS residual $|\psi_i|$ will exponentially converge to zero during Case 1. However, during Cases 2 and 3, the generated V2I IS residual $|\psi_i|$ will cross the threshold \mathcal{J}_{IS} to create V2I attack flag. Furthermore, similar to the V2X DS, the V2I IS gain matrix \mathfrak{M}_α , and the pre-defined threshold \mathcal{J}_{IS} can be designed by following steps described in Section 4.3-4.4. We point out here that for both the V2X DS and the V2I IS, the individual residual comparison enables the proposed algorithm to *identify the individual compromised vehicles* and thus, isolate the source of attacks.

Once the detection-isolation decision has been made, the system administrator can use an uncompromised channel or application to let the vehicles in the platoon know. At this stage, the platoon can disengage from standard driving and activate emergency “limp mode home” [61].

6 Simulation Results

In this section, we present the simulation results for a CAV platoon of 12 vehicles with one leader vehicle and 11 follower CAVs. Furthermore, we consider two different driving environments for the platoon, namely, highway driving and urban driving. To simulate the highway driving scenario, we extracted data for vehicle Id 1067 from NGSIM data and for the urban driving scenario, we utilized the UDDS data.

Next, for the follower vehicles of the platoon, we choose the engine dynamics time constant to be $\Sigma = 0.1s$. For nominal highway driving the vehicle controllers have gain values $k_1 = [0.2 \ 1 \ 2]$ and the desired time-headway $\mathcal{T}_1 = 0.5s$. Similarly, for nominal urban driving, the vehicle controllers have gain values $k_2 = [0.2 \ 2 \ -0.6]$ and the desired time-headway $\mathcal{T}_2 = 1.2s$ which is larger than that of highway driving due to the frequent stop-and-go scenario. The detector gains, \mathcal{L}_1 and isolator gains, \mathfrak{M}_1 for highway driving environment we choose $\mathcal{L}_1 = \mathfrak{M}_1 = \begin{bmatrix} 3 & 0.2 & 5 & 0.9 \\ 3 & -0.2 & -0.5 & 0.8 \end{bmatrix}$ such that they ensure performance benchmarks. Similarly, for the urban driving

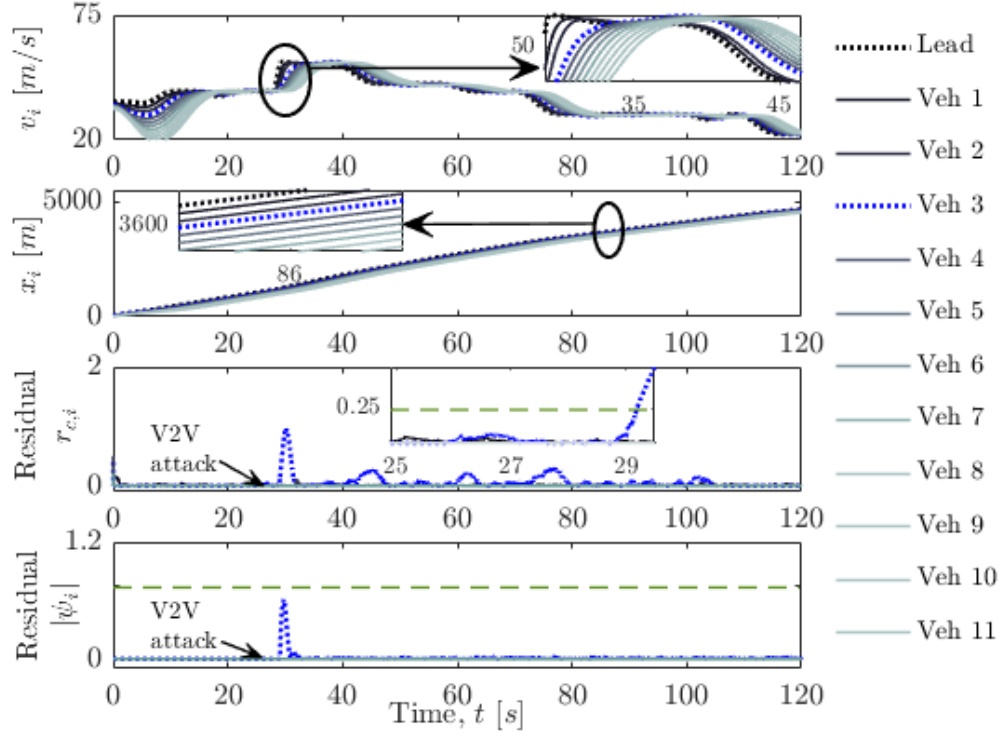


Figure 4: Under V2V cyberattack, the plot shows (top) the velocity, (second) the position, (third) the V2X DS residual, and (last) the V2I IS residual.

environment, are chosen to be $\mathcal{L}_2 = \mathfrak{M}_2 = \begin{bmatrix} 0.6 & 0.2 & 0.8 & 0.2 \\ 1.2 & 0.2 & 0.8 & 0.2 \end{bmatrix}$. Additionally, the system uncertainty is considered to be Gaussian i.e., $w_i \sim \mathcal{N}(0, 1)[1, 1]$ with maximum $\pm 5\%$ of velocity. The values of the thresholds \mathcal{J}_{DS} , and \mathcal{J}_{IS} are chosen to be 0.25 and 0.75 respectively. Now, we craft three attack scenarios to capture the various CAV attack complexities and variabilities such as single or multiple vehicle disruptions, different driving conditions, potentially disastrous consequences, and all possible cases of network corruption, i.e. only V2V, only V2I, and V2X attacks.

6.1 Replay attack on single vehicle through V2V network

First, we simulate the only V2V attack scenario ($f_{\theta i} \neq 0$, $f_{\alpha i}$, $f_{\theta \alpha i} = 0$) on the vehicle platoon running in a highway scenario. The V2V attack impacts the 3rd vehicle, i.e., the V2V communication between the 2nd vehicle and the 3rd vehicle has been compromised. The adversary first records u_2 signal from 18th s to 25th s and then starts to repeatedly send this 7s-long signal to the 3rd vehicle from 25th s. Thus, the 3rd vehicle effectively tracks the wrong desired acceleration leading to string instability [62]. This is evident from the top two plots of Fig. 4 (especially the zoomed inset plots) showing the position and velocity of the vehicles in the platoon. Now, the V2X detector can detect the attack on this platoon within 5s as the 3rd vehicle V2X DS residual $r_{c,3}$ crosses the threshold as shown in the third plot of Fig. 4. After a V2X detection, the 3rd V2I isolator is activated. However, since the platoon is under a V2V attack, the V2I IS residual $|\psi_3|$ remains under the threshold for all time (last plot in Fig. 4).

6.2 FDI attack on single vehicle through V2I network

Here we simulate the platoon running in a highway scenario under the only V2I attack scenario ($f_{\alpha i} \neq 0$, $f_{\theta i}$, $f_{\theta \alpha i} = 0$) which impacts the 8th vehicle from $t = 20$ s. In this FDI attack, the controller mode signal is α altered such that the 8th vehicle effectively runs with the controller gains and the desired headway for the urban driving environment. This causes the vehicle to lag behind the 7th vehicle further with time and ultimately CACC disengagement due to the vast distance from the preceding vehicle. The rest of the vehicles that are following the 8th vehicle are also disengaged. This is evident from the top two plots of Fig. 5 showing the position and velocity of the vehicles in the platoon, which is also expected from previous experimental studies [24]. Now, the V2X residual of the vehicle 8 $r_{c,8}$ crosses the

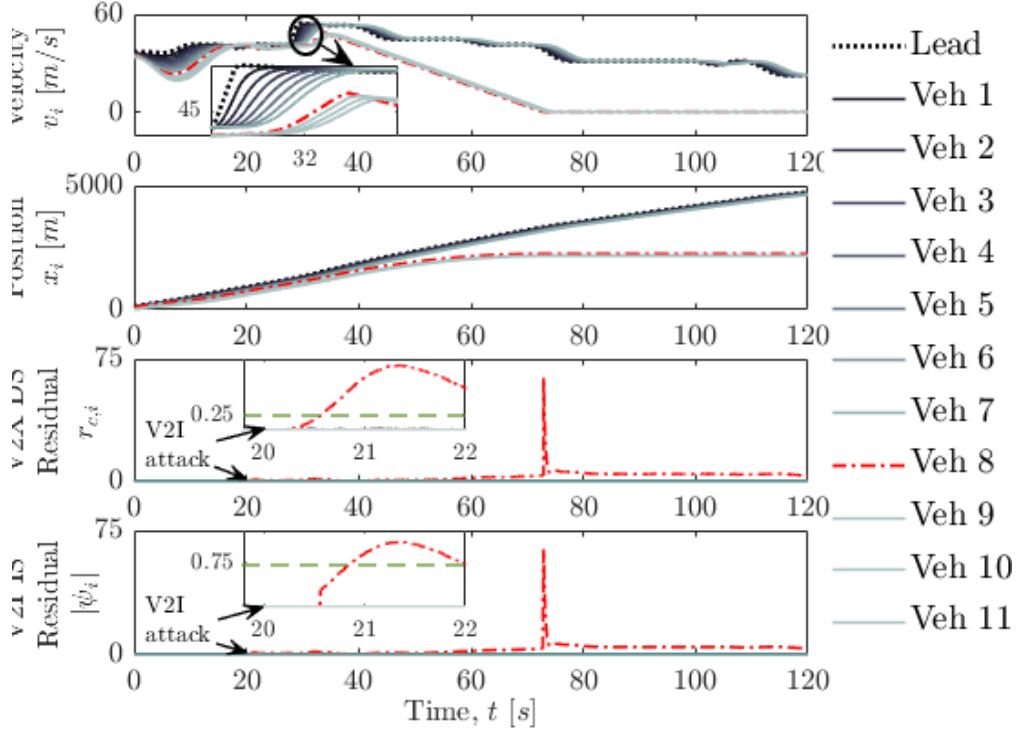


Figure 5: Under V2I cyberattack, the plot shows (top) the velocity, (second) the position, (third) the V2X DS residual, and (last) the V2I IS residual.

threshold within 2s of attack occurrence to accurately detect the attack as shown in the third plot of Fig. 5. After a V2X detection, the 8th V2I isolator is activated. Furthermore, as the platoon is under V2I attack, the V2I IS residual $|\psi_8|$ crosses the threshold confirming the presence of the V2I attack within 2s of activation. This is shown in the last plot in Fig. 5.

6.3 DDoS & FDI attacks on multiple vehicles through V2V-V2I networks

Lastly, we simulate the vehicle platoon under the simultaneous V2V-V2I attack scenario ($f_{\theta_i}, f_{\alpha_i}, f_{\theta_{\alpha_i}} \neq 0$) running in an urban driving scenario. Firstly, the adversary injects the DDoS attack on the V2V network of the 5th to 7th follower vehicles to disconnect them. Next, the adversary injects an FDI attack on the V2I network of the 6th vehicle. The V2V and V2I attacks are injected at $t = 25s$ and these lead to string instability and a rear-end collision scenario which is clearly evident in the first two plots of Fig. 6 showing the position and velocity of the vehicles in the platoon. Particularly, the zoomed portion of the velocity and position trajectory indicates the high probability of rear-end collisions. Furthermore, the V2X detector can detect the presence of the cyberattacks within 4s and activates corresponding isolators as shown in Fig. 6. Then the 6th V2I IS residual $|\psi_6|$ crosses the threshold and generates the V2I attack flag for this vehicle within 2s of activation. On the other hand, $|\psi_5|$, & $|\psi_7|$ remain below the threshold since only the V2V network is compromised for these vehicles. This is shown in the last plot of Fig. 6.

6.4 Attack sensitivity and statistical significance

Reliable V2X attack detection and V2I attack isolation under several presently prevalent cyberattacks on the real-world NGSIM and UDDS data demonstrate the efficacy of the proposed algorithm in a practical setting. Next, to further evaluate the effectiveness of the algorithm at the chosen threshold levels under diverse attack intensities we perform a Monte Carlo simulation of 720 test runs on the algorithm and obtain the receiver operating characteristics or ROC curve. The algorithm exhibits an optimal balance between the attack sensitivity and the robustness (detection probability and false alarm probability) at the chosen thresholds \mathcal{J}_{DS} and \mathcal{J}_{IS} as shown in the left plot of the Fig 7. Furthermore, the right plot in Fig 7 exhibits that on average, the algorithm can reliably detect the presence of the

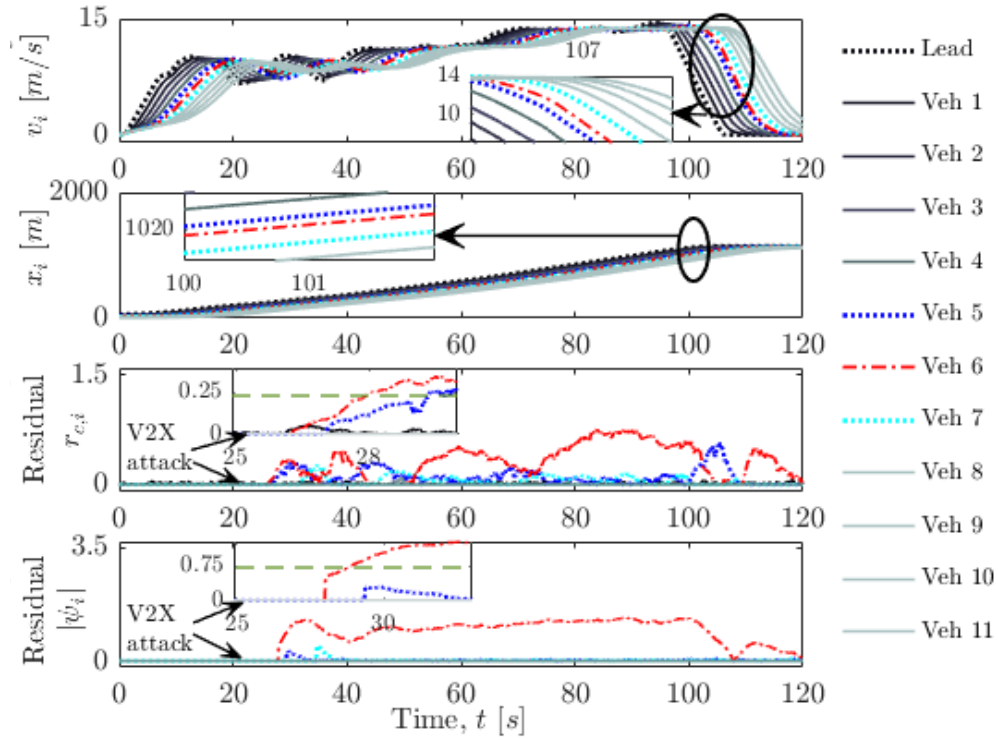


Figure 6: Under V2X cyberattack, the plot shows (top) the velocity, (second) the position, (third) the V2X DS residual, and (last) the V2I IS residual.

cyberattacks within 11 seconds of occurrence. However, low-impact attacks may remain undetected by the proposed algorithm leading to the 93% detection probability at the chosen threshold \mathcal{J}_{DS} .

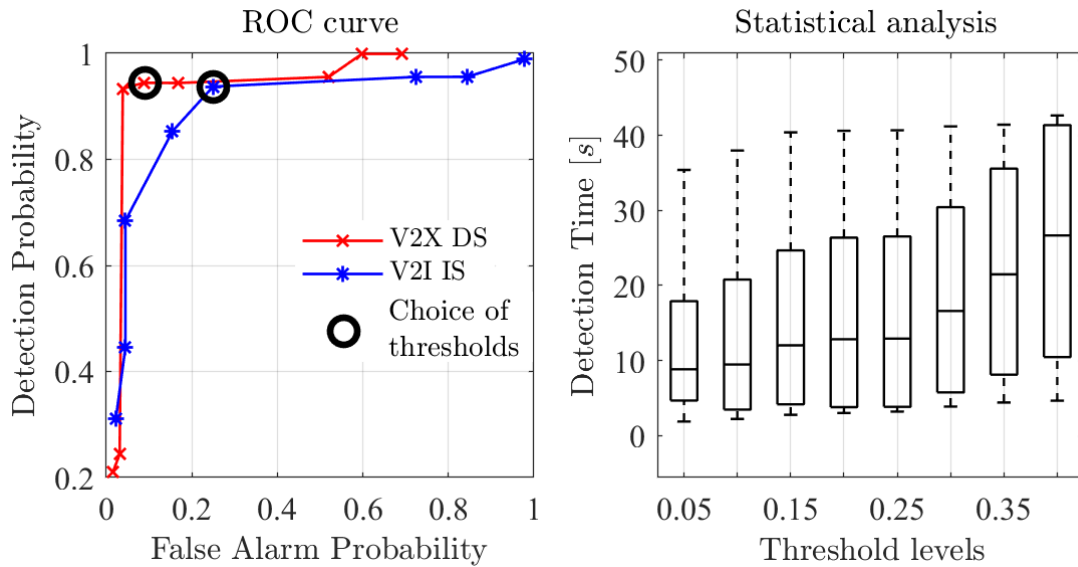


Figure 7: Plots exhibit algorithm performance under diverse attack intensities at different threshold settings: (left) Receiver Operating Characteristics or ROC curve and (right) Statistical analysis of detection time.

7 Conclusion

In summary, we proposed a two-phase VANET cyberattack detection-isolation algorithm to first detect cyberattacks and thereafter isolate the presence of V2I attacks for a CAV platoon. We considered multiple operational modes for the vehicle platoon in order to accommodate the changing driving environments of the platoon. Additionally, these model-based detectors and isolators were designed to ensure DSS with optimal robustness and sensitivity guarantees. Furthermore, we demonstrated the effectiveness of our algorithm using simulation case studies for three attack scenarios: only V2V, only V2I, and simultaneous V2V-V2I. The CAV driving environments were simulated here using UDDS and NGSIM data along with common cyberattacks such as DDoS, FDI, and replay attacks. In these case studies, our proposed algorithm successfully detected vehicular cyberattacks and isolated vehicles under a V2I attack. While additional experiments are needed in CAV testbeds before practical adoption and further analysis may be required to reevaluate the algorithm performance, if and when a new attack pattern emerges in the future, such detection decisions will ultimately help traffic administrators to employ steps towards damage mitigation while V2I attack isolation will help to secure central infrastructure access.

APPENDIX

Constants utilized in DSS criteria analysis	
$\beta_{6i} = \frac{\beta_{1i}}{\lambda_{\min}[N^T N]}$	$\bar{\beta}_{Fi} = \max[\beta_{2i}, \beta_{3i}, \beta_{4i}]$
$\gamma_{Fi} = \frac{\beta_{Fi}}{\gamma_{2i} \lambda_{\min}[P_\alpha]}$	$\ F_i\ _2^2 = \ f_{\alpha i}\ _2^2 + \ f_{\theta i}\ _2^2 + \ f_{\theta \alpha i}\ _2^2$
$\gamma_P = \frac{\lambda_{\max}[P_\alpha]}{\lambda_{\min}[P_\alpha]}$	$\gamma_{2i} = -\min_{\alpha} \frac{\lambda_{\min}[\Lambda_{2\alpha i}]}{\lambda_{\min}[\mathfrak{N}]}$
$\gamma_{wi} = \frac{\beta_{5i}}{\gamma_{2i} \lambda_{\min}[P_\alpha]}$	$\gamma_i = \frac{\beta_{6i} \gamma_P}{(\gamma_{2i} + \gamma_{2i-1}) \lambda_{\min}[P_\alpha]}$
$\mathfrak{P}_i = \max_{l \in \{1, \dots, i\}} [\gamma_l, \gamma_{Fl}, \gamma_{wl}] \prod_{k=l+1}^i \frac{\beta_{6k}}{\gamma_{2k} \lambda_{\min}[P_\alpha]}$	

Table 2: List of required constants

Proof of Theorem 1: Let us consider a family of Lyapunov functions for the switching-mode detector dynamics (15) as:

$$\Gamma_{\alpha i} = r_i^T P_\alpha r_i = e_i^T N^T P_\alpha N e_i = e_i \mathfrak{N} e_i, \quad (25)$$

where $P_\alpha \in \mathcal{P}$. Differentiating the Lyapunov function with respect to time we obtain

$$\begin{aligned} \dot{\Gamma}_{\alpha i} = & e_i^T \Lambda_{1\alpha i} e_i + q(e_i, \mathfrak{N} D_{\theta \alpha}, e_{i-1}) \\ & + q(e_i, \mathfrak{N} E_{\alpha i}, f_{\alpha i}) + q(e_i, \mathfrak{N} E_{\theta i}, f_{\theta i}) \\ & + q(e_i, \mathfrak{N} E_{\theta \alpha i}, f_{\theta \alpha i}) + q(e_i, \mathfrak{N}, w_i). \end{aligned} \quad (26)$$

Now, utilizing the Lyapunov function, we will prove the theorem in three parts:- DSS, robustness, and sensitivity.

DSS: The proposed detectors (15) are considered DSS, if for the vehicle platoon dynamics (14) under cyberattacks and uncertainties (i.e., $f_{\alpha i}, f_{\theta i}, f_{\theta \alpha i}, w_i \neq 0$) the generated V2X DS residual stays bounded, i.e. $r_{c,i} < \infty, \forall i \in \{1, \dots, n\}$. Before presenting the analysis, we present the definition of the required constants in the Table below.

Now, for $f_{\alpha i}, f_{\theta i}, f_{\theta \alpha i}, w_i \neq 0$, we have the derivative of $\Gamma_{\alpha i}$ from (26). Then, using the formula $X^T Y + Y^T X \leq \beta X^T X + \frac{1}{\beta} Y^T Y$, for $\beta > 0$, we can write (26) as

$$\begin{aligned} \dot{\Gamma}_{\alpha i} \leq & e_i^T \Lambda_{2\alpha i} e_i + \beta_{1i} \|e_{i-1}\|_2^2 + \beta_{2i} \|f_{\alpha i}\|_2^2 + \beta_{3i} \|f_{\theta i}\|_2^2 \\ & + \beta_{4i} \|f_{\theta \alpha i}\|_2^2 + \beta_{5i} \|w_i\|_2^2, \end{aligned} \quad (27)$$

where $\Lambda_{2\alpha i}$ is defined in Table 1. Next, from (17), we can write $\lambda_{\min}[N^T N] \|e_{i-1}\|_2^2 \leq \|r_{i-1}\|_2^2$. Furthermore, we obtain $e_i^T \Lambda_{2\alpha i} e_i \leq -\lambda_{\min}[\Lambda_{2\alpha i}] \|e_i\|_2^2$, for $\Lambda_{2\alpha i} < 0$. Similarly, from (25) we can deduce $\Gamma_{\alpha i} \geq \lambda_{\min}[\mathfrak{N}] \|e_i\|_2^2$. Thus, using $\gamma_{2i}, \beta_{6i}, \bar{\beta}_{Fi}$, and $\|F_i\|_2^2$ defined in Table 2, (27) can be rewritten as

$$\dot{\Gamma}_{\alpha i} \leq -\gamma_{2i} \Gamma_{\alpha i} + \beta_{6i} \|r_{i-1}\|_2^2 + \bar{\beta}_{Fi} \|F_i\|_2^2 + \beta_{5i} \|w_i\|_2^2. \quad (28)$$

The presence of r_{i-1} in (28), shows that the cumulative impact of all the preceding vehicles, $\{0, 1, \dots, i-1\}$ is embedded in the i^{th} detector. Thus, we proceed to prove this recursively. First, we prove for $i = 1$. We note here, for the leader vehicle i.e., $i = 0$, the full state is known to V2X DS from GNSS data (since $u_0 = a_0$), and thus the

error $e_0 = \zeta_0 - \hat{\zeta}_0 = 0$. Therefore, from (17) we obtain $\|r_0\|_2^2 \leq \lambda_{\max}[N^T N] \|e_0\|_2^2 = 0$. Hence, for $i = 1$, applying Gronwall's inequality on (28)

$$\Gamma_{\alpha 1}(t) \leq \Gamma_{\alpha 1}(0)e^{-\gamma_{21}t} + \frac{\bar{\beta}_{F1}}{\gamma_{21}} \|F_1\|_{\mathcal{L}_2}^2 + \frac{\beta_{51}}{\gamma_{21}} \|w_1\|_{\mathcal{L}_2}^2. \quad (29)$$

Then, using (25), we can write $\lambda_{\min}[P_{\alpha}] \|r_1(t)\|_2^2 \leq \Gamma_{\alpha 1}(t)$ and $\Gamma_{\alpha 1}(0) \leq \lambda_{\max}[P_{\alpha}] \|r_1(0)\|_2^2$. Thus, we utilize the variables defined in Table 2 for $i = 1$ such that we re-write (29) as

$$\|r_1(t)\|_2^2 \leq \gamma_P \|r_1(0)\|_2^2 e^{-\gamma_{21}t} + \gamma_{F1} \|F_1\|_{\mathcal{L}_2}^2 + \gamma_{w1} \|w_1\|_{\mathcal{L}_2}^2.$$

With this, we prove that detector 1 is DSS. Henceforth, and using (28) for $i = 2$ we obtain

$$\begin{aligned} \dot{\Gamma}_{\alpha 2} &\leq -\gamma_{22} \Gamma_{\alpha 2} + \bar{\beta}_{F2} \|F_2\|_2^2 + \beta_{52} \|w_2\|_2^2 + \beta_{62} \\ &\quad [\gamma_P \|r_1(0)\|_2^2 e^{-\gamma_{21}t} + \gamma_{F1} \|F_1\|_{\mathcal{L}_2}^2 + \gamma_{w1} \|w_1\|_{\mathcal{L}_2}^2]. \end{aligned} \quad (30)$$

Following similar steps after applying Gronwall's inequality and using γ_2 from Table 2 we obtain

$$\begin{aligned} \|r_2(t)\|_2^2 &\leq \gamma_P \|r_2(0)\|_2^2 e^{-\gamma_{22}t} + \gamma_2 \|r_1(0)\|_{\mathcal{L}_2}^2 + \gamma_{F2} \|F_2\|_{\mathcal{L}_2}^2 \\ &\quad + \gamma_{w2} \|w_2\|_{\mathcal{L}_2}^2 + \frac{\beta_{62}}{\gamma_{22} \lambda_{\min}[P_{\alpha}]} [\gamma_{F1} \|F_1\|_{\mathcal{L}_2}^2 + \gamma_{w1} \|w_1\|_{\mathcal{L}_2}^2]. \end{aligned}$$

Thus, for \mathfrak{P}_i from Table 2, iteratively it can be shown that

$$\begin{aligned} \|r_i(t)\|_2^2 &\leq \gamma_P \|r_i(0)\|_2^2 e^{-\gamma_{2i}t} + \\ &\quad \mathfrak{P}_i \sum_{l=1}^i [\|r_{l-1}(0)\|_{\mathcal{L}_2}^2 + \|F_l\|_{\mathcal{L}_2}^2 + \|w_l\|_{\mathcal{L}_2}^2]. \end{aligned} \quad (31)$$

With this, we prove DSS criteria for r_i . Furthermore, this implies that r_{i-1} and subsequently e_{i-1} is also bounded under the presence of cyberattack and uncertainty since from (17) we can write $\lambda_{\min}[N^T N] \|e_{i-1}\|_2^2 \leq \|r_{i-1}\|_2^2$. If r_i is greater than e_{i-1} then $\|r_i\|_2^2 - \|e_{i-1}\|_2^2$ is positive and less than r_i . This implies that under this condition $r_{c,i}$ is less than equal to the right-hand-side (RHS) of (31). Moreover, if r_i is less than e_{i-1} , $r_{c,i} = 0$. However, the RHS of (31) is always non-negative, which implies for the r_i less than e_{i-1} case, then $r_{c,i}$ is still less than equal to the RHS of (31). This yields

$$\begin{aligned} r_{c,i} &\leq \gamma_P \|r_i(0)\|_2^2 e^{-\gamma_{2i}t} + \mathfrak{P}_i \sum_{l=1}^i [\|r_{l-1}(0)\|_{\mathcal{L}_2}^2 \\ &\quad + \|f_{\alpha l}\|_{\mathcal{L}_2}^2 + \|f_{\theta l}\|_{\mathcal{L}_2}^2 + \|f_{\theta \alpha l}\|_{\mathcal{L}_2}^2 + \|w_l\|_{\mathcal{L}_2}^2]. \end{aligned} \quad (32)$$

This ensures the DSS criteria for the proposed detector (15).

Robustness: The i^{th} detector is considered robust towards uncertainties ($w_i \neq 0$), if under no cyberattack ($f_{\alpha i}, f_{\theta i}, f_{\theta \alpha i} = 0$) the V2X DS residual $r_{c,i}(t)$ does not cross a predefined threshold value. Thus, the detector is robust if there exists RF, $\rho_{1i} > 0$ such that $\forall i \in \{1, \dots, n\}$

$$\int_0^\infty r_{c,i} dt \leq \rho_{1i} \int_0^\infty \|w_i\|_2^2 dt + \epsilon_1. \quad (33)$$

Furthermore, the non-negative RHS of the inequality in (33) implies that proving $\|r_i\|_2^2 - \|e_{i-1}\|_2^2$ is smaller than the RHS will prove each component of $r_{c,i}$ (18) is individually less than the RHS. Therefore, it is sufficient to prove

$$\int_0^\infty [\|r_i\|_2^2 - \|e_{i-1}\|_2^2] dt \leq \rho_{1i} \int_0^\infty \|w_i\|_2^2 dt + \epsilon_1, \quad (34)$$

to ensure robustness. First, let us define a vector $\chi_{1i} = [r_i^T \quad e_{i-1}^T \quad w_i^T]^T$. Now, the robustness criteria from (34) can be re-written using the definition of \mathcal{G}_1 , from Table 1 as $\int_0^\infty \chi_{1i}^T \mathcal{G}_1 \chi_{1i} dt - \epsilon_1 \leq 0$. Next, let us consider the same Lyapunov function from (25). Since $f_{\alpha i}, f_{\theta i}, f_{\theta \alpha i} = 0, w_i \neq 0$ for this criteria, the derivative of $\Gamma_{\alpha i}$ is modified to $\dot{\Gamma}_{\alpha i} \leq \chi_{1i}^T \mathcal{B}_{1\alpha i} \chi_{1i}$ using (26), where $\mathcal{B}_{1\alpha i}$, is defined in Table 1. Thus, integrating this inequality we obtain

$$\Gamma_{\alpha i}(\infty) - \Gamma_{\alpha i}(0) - \int_0^\infty \chi_{1i}^T \mathcal{B}_{1\alpha i} \chi_{1i} dt \leq 0. \quad (35)$$

Since the left-hand-side (LHS) of the (35) is non-positive, if $\int_0^\infty \chi_{1i}^T \mathcal{G}_1 \chi_{1i} dt - \epsilon_1$ can be proved to be smaller than the LHS of the (35), then $\int_0^\infty \chi_{1i}^T \mathcal{G}_1 \chi_{1i} dt - \epsilon_1$ will also be non-positive. Mathematically, it implies that we can prove

$$\int_0^\infty \chi_{1i}^T \mathcal{G}_1 \chi_{1i} dt - \epsilon_1 \leq \Gamma_{\alpha i}(\infty) - \Gamma_{\alpha i}(0) - \int_0^\infty \chi_{1i}^T \mathcal{B}_{1\alpha i} \chi_{1i} dt,$$

to prove (34). This condition can be further modified as

$$\int_0^\infty \chi_{1i}^T [\mathcal{G}_1 + \mathcal{B}_{1\alpha i}] \chi_{1i} dt \leq \Gamma_{\alpha i}(\infty) - \Gamma_{\alpha i}(0) + \epsilon_1. \quad (36)$$

Now, by definition $\Gamma_{\alpha i}(\infty) \geq 0$. Using (25), we can write $\Gamma_{\alpha i}(0) = r_i^T(0) P_\alpha r_i(0) \leq \lambda_{\max}[P_\alpha] \max_i \|r_i(0)\|_2^2$. Thus, we can deduce $\Gamma_{\alpha i}(0) - \epsilon_1 \leq 0$ for $\epsilon_1 \geq \lambda_{\max}[P_\alpha] \max_i \|r_i(0)\|_2^2$. Therefore, we can write

$$\Gamma_{\alpha i}(\infty) - \Gamma_{\alpha i}(0) + \epsilon_1 \geq 0. \quad (37)$$

Hence, if we can guarantee

$$\int_0^\infty \chi_{1i}^T [\mathcal{G}_1 + \mathcal{B}_{1\alpha i}] \chi_{1i} dt \leq 0, \quad (38)$$

then it will be sufficient to prove (36) using (37). (38) thus provides us with the LMI criteria $\mathcal{G}_1 + \mathcal{B}_{1\alpha i} \leq 0$ that proves (36) which is equivalent to prove (34). Thus, we prove that (21) is a sufficient condition for guaranteeing robustness.

Sensitivity: In the presence of cyberattacks and no uncertainties, a detector is considered sensitive towards cyberattack if the V2X DS residual $r_{c,i}(t)$ can cross a predefined threshold value regardless of the amplitude of the attack. Furthermore, from (18), we can write $r_{c,i} \geq \|r_i\|_2^2 - \|e_{i-1}\|_2^2$. Thus, for $f_{\alpha i}, f_{\theta i}, f_{\theta \alpha i} \neq 0$ and $w_i = 0$, the detector is sensitive if there exists SF, $\rho_{2i} > 0$ and $\epsilon_1 > 0$, such that $\forall i \in \{1, \dots, n\}$

$$\begin{aligned} \int_0^\infty r_{c,i} dt &\geq \int_0^\infty [\|r_i\|_2^2 - \|e_{i-1}\|_2^2] dt \geq \\ \rho_{2i} \int_0^\infty [\|f_{\alpha i}\|_2^2 + \|f_{\theta i}\|_2^2 + \|f_{\theta \alpha i}\|_2^2] dt &- \epsilon_1. \end{aligned} \quad (39)$$

Hence, we note that to prove the sensitivity condition it is adequate to prove the second inequality in (39). Now, for design flexibility we substitute $\rho_{2i} = \frac{\rho_{4i}}{\rho_{3i}}$ in (39) to get

$$\rho_{3i} \int_0^\infty [\|r_i\|_2^2 - \|e_{i-1}\|_2^2] dt \geq \rho_{4i} \int_0^\infty \|F_i\|_2^2 dt - \epsilon_2, \quad (40)$$

where $\epsilon_2 = \rho_{3i} \epsilon_1$, and $\|F_i\|_2^2$ is defined in Table 2. Now to prove this, let us define another vector $\chi_{2i} = [r_i^T \ e_{i-1}^T \ f_{\alpha i}^T \ f_{\theta i}^T \ f_{\theta \alpha i}^T]^T$. Next, using the definition of \mathcal{G}_2 from Table 1, (40) can be re-written as:

$$\int_0^\infty \chi_{2i}^T \mathcal{G}_2 \chi_{2i} dt + \epsilon_2 \geq 0. \quad (41)$$

Then considering the same Lyapunov functions defined in (25) under $f_{\alpha i}, f_{\theta i}, f_{\theta \alpha i} \neq 0$ and $w_i = 0$, the derivative of $\Gamma_{\alpha i}$ from (26) can be modified as $\dot{\Gamma}_{\alpha i} \leq \chi_{2i}^T \mathcal{B}_{2\alpha i} \chi_{2i}$, where $\mathcal{B}_{2\alpha i}$ is defined in Table 1. We note here that to obtain this inequality we have utilized the fact, for $\gamma_{1i} > 0$, $\gamma_{1i} r_i^T r_i \geq -\gamma_{1i} r_i^T r_i$. Next, we integrate the inequality to get

$$\int_0^\infty \chi_{2i}^T \mathcal{B}_{2\alpha i} \chi_{2i} dt - \Gamma_{\alpha i}(\infty) + \Gamma_{\alpha i}(0) \geq 0. \quad (42)$$

Since LHS of (42) is positive, if $\int_0^\infty \chi_{2i}^T \mathcal{G}_2 \chi_{2i} dt + \epsilon_2$ can be proved to be larger than the LHS of (42), then $\int_0^\infty \chi_{2i}^T \mathcal{G}_2 \chi_{2i} dt + \epsilon_2$ will also be positive. This implies that we must prove

$$\int_0^\infty \chi_{2i}^T \mathcal{G}_2 \chi_{2i} dt + \epsilon_2 \geq \int_0^\infty \chi_{2i}^T \mathcal{B}_{2\alpha i} \chi_{2i} dt - \Gamma_{\alpha i}(\infty) + \Gamma_{\alpha i}(0),$$

to prove (41). This inequality condition can be rearranged as

$$\int_0^\infty \chi_{2i}^T [\mathcal{G}_2 - \mathcal{B}_{2\alpha i}] \chi_{2i} dt \geq \Gamma_{\alpha i}(0) - \epsilon_2 - \Gamma_{\alpha i}(\infty). \quad (43)$$

Furthermore, from (37), we can write $\Gamma_{\alpha_i}(0) - \epsilon_2 - \Gamma_{\alpha_i}(\infty) \leq 0$ for $\epsilon_2 \geq \lambda_{\max}[P_{\alpha_i}] \max_i \|r_i(0)\|_2^2$. Consequently, we can deduce that when $\int_0^\infty \chi_{2i}^T [\mathcal{G}_2 - \mathcal{B}_{2\alpha_i}] \chi_{2i} dt$ is positive, then the inequality (43) will be satisfied. Thus, if we can guarantee

$$\int_0^\infty \chi_{2i}^T [\mathcal{G}_2 - \mathcal{B}_{2\alpha_i}] \chi_{2i} dt \geq 0, \quad (44)$$

it will prove (43) which in turn proves (40). Therefore, (44) implies that the LMI condition proposed in (22), i. e. $[\mathcal{G}_2 - \mathcal{B}_{2\alpha_i}] \geq 0$ is a sufficient condition to ensure the sensitivity of the proposed V2X DS.

We note here that Sylvester's criterion for $[\mathcal{G}_2 - \mathcal{B}_{2\alpha_i}] \geq 0$ requires \mathfrak{L}_α to be chosen such that $\gamma_{1_i} = \rho_{3_i}$. Now, if we had not introduced ρ_{3_i}, ρ_{4_i} in (40), it would require $\gamma_{1_i} = 1$ which significantly constrains the design freedom. Therefore, to attain more design flexibility, we introduced parameters ρ_{3_i}, ρ_{4_i} in place of ρ_{2_i} using Table 1.

Optimization: So far, we proved that satisfying the criteria (20)-(22) ensures DSS, robustness, and sensitivity of the proposed detector. Next, to achieve an optimal trade-off between robustness and sensitivity, we utilize the constrained multi-objective optimization problem established in (19) that optimally minimizes ρ_{1_i} while maximizing ρ_{2_i} over \mathfrak{L}_α . The choice of weight vector μ_i depends on system-specific robustness and sensitivity requirements. The optimizer will be more biased towards sensitivity than robustness for $\mu_i < 0.5$ and vice versa. The constraints of the optimization problem, i. e., the LMIs (20), (21), and (22) are respectively the sufficient conditions for DSS, robustness, and sensitivity of the detection scheme. Therefore, the solution of the optimization problem established in (19) gives the gain matrices that ensure the benchmark performance of the proposed V2X DS. ■

References

- [1] Todd Litman. *Autonomous vehicle implementation predictions*. Victoria Transport Policy Institute Victoria, BC, Canada, 2017.
- [2] Kakan C Dey, Li Yan, Xujie Wang, Yue Wang, Haiying Shen, Mashrur Chowdhury, Lei Yu, Chenxi Qiu, and Vivekgautham Soundararaj. A review of communication, driver characteristics, and controls aspects of cooperative adaptive cruise control (CACC). *IEEE Transactions on Intelligent Transportation Systems*, 17(2):491–509, 2015.
- [3] Connected vehicles and cybersecurity, 2023.
- [4] Franco van Wyk, Yiyang Wang, Anahita Khojandi, and Neda Masoud. Real-time sensor anomaly detection and identification in automated vehicles. *IEEE Transactions on Intelligent Transportation Systems*, 21(3):1264–1276, 2020.
- [5] Ian Ku, You Lu, Mario Gerla, Rafael L. Gomes, Francesco Ongaro, and Eduardo Cerqueira. Towards software-defined VANET: Architecture and services. In *2014 13th Annual Mediterranean Ad Hoc Networking Workshop (MED-HOC-NET)*, pages 103–110, 2014.
- [6] Mikhail Buinevich and Andrei Vladyko. Forecasting issues of wireless communication networks' cyber resilience for an intelligent transportation system: An overview of cyber attacks. *Information*, 10(1):27, 2019.
- [7] Zhiyang Ju, Hui Zhang, Xiang Li, Xiaoguang Chen, Jinpeng Han, and Manzhi Yang. A survey on attack detection and resilience for connected and automated vehicles: From vehicle dynamics and control perspective. *IEEE Transactions on Intelligent Vehicles*, 7(4):815–837, 2022.
- [8] Sanchita Ghosh and Tanushree Roy. Security of cyber-physical systems under compromised switching. In *2023 IEEE Conference on Control Technology and Applications (CCTA)*, pages 1034–1039. IEEE, 2023.
- [9] DVAHG Swaroop and R Huandra. Intelligent cruise control system design based on a traffic flow specification. *Vehicle system dynamics*, 30(5):319–344, 1998.
- [10] Qing Xu and Raja Sengupta. Simulation, analysis, and comparison of ACC and CACC in highway merging control. In *IEEE IV2003 Intelligent Vehicles Symposium. Proceedings (Cat. No. 03TH8683)*, pages 237–242. IEEE, 2003.
- [11] Ali Balador, Alessandro Bazzi, Unai Hernandez-Jayo, Idoia de la Iglesia, and Hossein Ahmadvand. A survey on vehicular communication for cooperative truck platooning application. *Vehicular Communications*, page 100460, 2022.
- [12] Ke Song, Feiqiang Li, Xiao Hu, Lin He, Wenxu Niu, Sihao Lu, and Tong Zhang. Multi-mode energy management strategy for fuel cell electric vehicles based on driving pattern identification using learning vector quantization neural network algorithm. *Journal of Power Sources*, 389:230–239, 2018.

- [13] Chan-Chiao Lin, Soonil Jeon, Hwei Peng, and Jang Moo Lee. Driving pattern recognition for control of hybrid electric trucks. *Vehicle System Dynamics*, 42(1-2):41–58, 2004.
- [14] R. Langari and Jong-Seob Won. Intelligent energy management agent for a parallel hybrid vehicle-part I: system architecture and design of the driving situation identification process. *IEEE Transactions on Vehicular Technology*, 54(3):925–934, 2005.
- [15] Soon-il Jeon, Sung-tae Jo, Yeong-il Park, and Jang-moo Lee. Multi-mode driving control of a parallel hybrid electric vehicle using driving pattern recognition. *J. Dyn. Sys., Meas., Control*, 124(1):141–149, 2002.
- [16] Eleonora D’Andrea, Pietro Ducange, Beatrice Lazzerini, and Francesco Marcelloni. Real-time detection of traffic from twitter stream analysis. *IEEE Transactions on Intelligent Transportation Systems*, 16(4):2269–2283, 2015.
- [17] Bo Chen and Harry H Cheng. A review of the applications of agent technology in traffic and transportation systems. *IEEE Transactions on intelligent transportation systems*, 11(2):485–497, 2010.
- [18] Gongjun Yan Yan, Gyanesh Choudhary, Michele C Weigle, and Stephan Olariu. Providing VANET security through active position detection. In *Proceedings of the fourth ACM international workshop on Vehicular ad hoc networks*, pages 73–74, 2007.
- [19] Hamssa Hasrouny, Abed Ellatif Samhat, Carole Bassil, and Anis Laouiti. VANet security challenges and solutions: A survey. *Vehicular Communications*, 7:7–20, 2017.
- [20] Mohammad Ali Salahuddin, Ala Al-Fuqaha, and Mohsen Guizani. Software-defined networking for RSU clouds in support of the internet of vehicles. *IEEE Internet of Things Journal*, 2(2):133–144, 2015.
- [21] John B. Kenney. Dedicated short-range communications (DSRC) standards in the united states. *Proceedings of the IEEE*, 99(7):1162–1182, 2011.
- [22] Fan Bai, Daniel D Stancil, and Hariharan Krishnan. Toward understanding characteristics of dedicated short-range communications (DSRC) from a perspective of vehicular network engineers. In *Proceedings of the sixteenth annual international conference on Mobile computing and networking*, pages 329–340, 2010.
- [23] Pengcheng Wang, Xinkai Wu, and Xiaozheng He. Modeling and analyzing cyberattack effects on connected automated vehicular platoons. *Transportation research part C: emerging technologies*, 115:102625, 2020.
- [24] George Gunter, Derek Gloudemans, Raphael E Stern, Sean McQuade, Rahul Bhadani, Matt Bunting, Maria Laura Delle Monache, Roman Lysecky, Benjamin Seibold, Jonathan Sprinkle, et al. Are commercially implemented adaptive cruise control systems string stable? *IEEE Transactions on Intelligent Transportation Systems*, 22(11):6992–7003, 2020.
- [25] Richard Gilles Engoulou, Martine Bellaïche, Samuel Pierre, and Alejandro Quintero. VANET security surveys. *Computer Communications*, 44:1–13, 2014.
- [26] Ahmed Shoeb Al Hasan, Md Shohrab Hossain, and Mohammed Atiquzzaman. Security threats in vehicular ad hoc networks. In *2016 international conference on advances in computing, communications and informatics (ICACCI)*, pages 404–411. IEEE, 2016.
- [27] Tanushree Roy, Sara Sattarzadeh, and Satadru Dey. Cyber-attack detection in socio-technical transportation systems exploiting redundancies between physical and social data. *arXiv preprint arXiv:2103.11422*, 2021.
- [28] Jack Reilly, Sébastien Martin, Mathias Payer, and Alexandre M Bayen. Creating complex congestion patterns via multi-objective optimal freeway traffic control with application to cyber-security. *Transportation Research Part B: Methodological*, 91:366–382, 2016.
- [29] Sanchita Ghosh and Tanushree Roy. Security of cyber-physical systems under compromised switching. In *2023 IEEE Conference on Control Technology and Applications (CCTA)*, pages 1034–1039. IEEE, 2023.
- [30] Mhafuzul Islam, Mashrur Chowdhury, Hongda Li, and Hongxin Hu. Cybersecurity attacks in vehicle-to-infrastructure applications and their prevention. *Transportation research record*, 2672(19):66–78, 2018.
- [31] Srivalli Boddupalli, Ashwini Hegde, and Sandip Ray. Replace: Real-time security assurance in vehicular platoons against v2v attacks. In *2021 IEEE International Intelligent Transportation Systems Conference (ITSC)*, pages 1179–1185, 2021.
- [32] Srivalli Boddupalli, Akash Someshwar Rao, and Sandip Ray. Resilient cooperative adaptive cruise control for autonomous vehicles using machine learning. *IEEE Transactions on Intelligent Transportation Systems*, 23(9):15655–15672, 2022.
- [33] Gurcan Comert, Mizanur Rahman, Mhafuzul Islam, and Mashrur Chowdhury. Change point models for real-time cyber attack detection in connected vehicle environment. *IEEE Transactions on Intelligent Transportation Systems*, 23(8):12328–12342, 2022.

- [34] Jinpeng Han, Zhiyang Ju, Xiaoguang Chen, Manzhi Yang, Hui Zhang, and Rouxing Huai. Secure operations of connected and autonomous vehicles. *IEEE Transactions on Intelligent Vehicles*, 2023.
- [35] Maxim Kalinin, Vasiliy Krundyshev, Peter Zegzhda, and Viacheslav Belenko. Network security architectures for VANET. In *Proceedings of the 10th International Conference on Security of Information and Networks*, pages 73–79, 2017.
- [36] Feng Jiang, Buren Qi, Tianhao Wu, Konglin Zhu, and Lin Zhang. CPSS: CP-ABE based platoon secure sensing scheme against Cyber-Attacks. In *2019 IEEE Intelligent Transportation Systems Conference (ITSC)*, pages 3218–3223, 2019.
- [37] Bin Xiao, Bo Yu, and Chuanshan Gao. Detection and localization of sybil nodes in VANETs. In *Proceedings of the 2006 workshop on Dependability issues in wireless ad hoc networks and sensor networks*, pages 1–8, 2006.
- [38] Seyhan Ucar, Sinem Coleri Ergen, and Ozgur Ozkasap. Data-driven abnormal behavior detection for autonomous platoon. In *2017 IEEE Vehicular Networking Conference (VNC)*, pages 69–72, 2017.
- [39] Philipp Mundhenk, Andrew Paverd, Artur Mrowca, Sebastian Steinhorst, Martin Lukasiewicz, Suhaib A Fahmy, and Samarjit Chakraborty. Security in automotive networks: Lightweight authentication and authorization. *ACM Transactions on Design Automation of Electronic Systems (TODAES)*, 22(2):1–27, 2017.
- [40] Qiao Yan, F Richard Yu, Qingxiang Gong, and Jianqiang Li. Software-defined networking (SDN) and distributed denial of service (DDoS) attacks in cloud computing environments: A survey, some research issues, and challenges. *IEEE communications surveys & tutorials*, 18(1):602–622, 2015.
- [41] Abdul Rehman Javed, Muhammad Usman, Saif Ur Rehman, Mohib Ullah Khan, and Mohammad Sayad Haghighi. Anomaly detection in automated vehicles using multistage attention-based convolutional neural network. *IEEE Transactions on Intelligent Transportation Systems*, 22(7):4291–4300, 2020.
- [42] Jingjing Guo, Xinghua Li, Zhiquan Liu, Jianfeng Ma, Chao Yang, Junwei Zhang, and Dapeng Wu. TROVE: A context-awareness trust model for VANETs using reinforcement learning. *IEEE Internet of Things Journal*, 7(7):6647–6662, 2020.
- [43] Hind Bangui, Mouzhi Ge, and Barbora Buhnova. A hybrid machine learning model for intrusion detection in VANET. *Computing*, 104(3):503–531, 2022.
- [44] Yuanzhe Wang, Qipeng Liu, Ehsan Mihankhah, Chen Lv, and Danwei Wang. Detection and isolation of sensor attacks for autonomous vehicles: Framework, algorithms, and validation. *IEEE Transactions on Intelligent Transportation Systems*, 23(7):8247–8259, 2022.
- [45] Jiaping Xiao and Mir Feroskhan. Cyber attack detection and isolation for a quadrotor UAV with modified sliding innovation sequences. *IEEE Transactions on Vehicular Technology*, 71(7):7202–7214, 2022.
- [46] Philipp Kremer, Ipsita Koley, Soumyajit Dey, and Sangyoung Park. State estimation for attack detection in vehicle platoon using VANET and controller model. In *2020 IEEE 23rd International Conference on Intelligent Transportation Systems (ITSC)*, pages 1–8. IEEE, 2020.
- [47] Yiyang Wang, Neda Masoud, and Anahita Khojandi. Anomaly detection in connected and automated vehicles using an augmented state formulation. In *2020 Forum on Integrated and Sustainable Transportation Systems (FISTS)*, pages 156–161, 2020.
- [48] Xingkang He, Ehsan Hashemi, and Karl H Johansson. Distributed control under compromised measurements: Resilient estimation, attack detection, and vehicle platooning. *Automatica*, 134:109953, 2021.
- [49] Eman Mousavinejad, Fuwen Yang, Qing-Long Han, Xiaohua Ge, and Ljubo Vlacic. Distributed cyber attacks detection and recovery mechanism for vehicle platooning. *IEEE Transactions on Intelligent Transportation Systems*, 21(9):3821–3834, 2020.
- [50] Tanushree Roy, Amara Tariq, and Satadru Dey. A socio-technical approach for resilient connected transportation systems in smart cities. *IEEE Transactions on Intelligent Transportation Systems*, 23(6):5019–5028, 2021.
- [51] Tianci Yang and Chen Lv. Secure estimation and attack isolation for connected and automated driving in the presence of malicious vehicles. *IEEE Transactions on Vehicular Technology*, 70(9):8519–8528, 2021.
- [52] Zoleikha Abdollahi Biron, Satadru Dey, and Pierluigi Pisù. Real-time detection and estimation of denial of service attack in connected vehicle systems. *IEEE Transactions on Intelligent Transportation Systems*, 19(12):3893–3902, 2018.
- [53] Chunjie Zhai, Yonggui Liu, and Fei Luo. A switched control strategy of heterogeneous vehicle platoon for multiple objectives with state constraints. *IEEE Transactions on Intelligent Transportation Systems*, 20(5):1883–1896, 2018.

- [54] Shengyue Yao, Rahi Avinash Shet, and Bernhard Friedrich. Managing connected automated vehicles in mixed traffic considering communication reliability: a platooning strategy. *Transportation Research Procedia*, 47:43–50, 2020.
- [55] Valerio Turri, Bart Besselink, and Karl H Johansson. Cooperative look-ahead control for fuel-efficient and safe heavy-duty vehicle platooning. *IEEE Transactions on Control Systems Technology*, 25(1):12–28, 2016.
- [56] Tanushree Roy and Satadru Dey. Secure traffic networks in smart cities: Analysis and design of cyber-attack detection algorithms. In *2020 American Control Conference (ACC)*, pages 4102–4107. IEEE, 2020.
- [57] Joao P Hespanha and A Stephen Morse. Stability of switched systems with average dwell-time. In *Proceedings of the 38th IEEE conference on decision and control (Cat. No. 99CH36304)*, volume 3, pages 2655–2660. IEEE, 1999.
- [58] Wenli Duo, MengChu Zhou, and Abdullah Abusorrah. A survey of cyber attacks on cyber physical systems: Recent advances and challenges. *IEEE/CAA Journal of Automatica Sinica*, 9(5):784–800, 2022.
- [59] Mashrur Chowdhury, Mhafuzul Islam, and Zadid Khan. Security of connected and automated vehicles. *arXiv preprint arXiv:2012.13464*, 2020.
- [60] Steven X Ding. Model-based fault diagnosis techniques: Design schemes, algorithms, and tools.
- [61] Ehsan Dehghan-Azad, Shady Gadoue, David Atkinson, Howard Slater, Peter Barrass, and Frede Blaabjerg. Sensorless control of im for limp-home mode ev applications. *IEEE Transactions on Power Electronics*, 32(9):7140–7150, 2016.
- [62] Jeroen Ploeg, Bart TM Scheepers, Ellen Van Nunen, Nathan Van de Wouw, and Henk Nijmeijer. Design and experimental evaluation of cooperative adaptive cruise control. In *2011 14th International IEEE Conference on Intelligent Transportation Systems (ITSC)*, pages 260–265. IEEE, 2011.